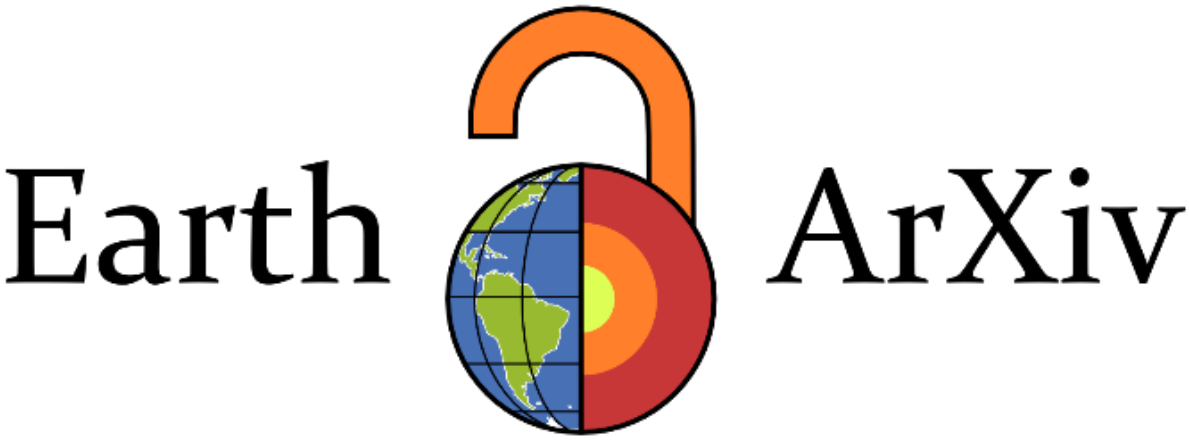

Missing well logs prediction method based on K-nearest neighbors regression

Ali Abdalsalam[1]

[1] Earth Science Department, Damanhour University, Damanhour, 22516, Egypt (E-mail: alialiabdalsalam@gmail.com)

Corresponding Authors:
Ali Abdalsalam[1]
Earth Science Department, Damanhour University, Damanhour, 22516, Egypt
Email address: alialiabdalsalam@gmail.com

Abstract

In petroleum exploration, well logs are crucial for reservoir characterization. However, missing well logs frequently occur due to tool failures or economic constraints, which can impede accurate subsurface modeling. This research presents a method for predicting missing well logs using the K-Nearest Neighbors (KNN) regression algorithm, trained on data from the University of Kansas. The study focuses on predicting Delta T (DT) and Gamma Ray (GR) logs across five wells. The KNN model effectively captures the relationships between available and missing logs through proximity-based predictions, leveraging patterns from similar well-log data. The model achieved high test accuracy with R^2 scores ranged from 0.942 to 0.963 for DT and 0.927 to 0.930 for GR, indicating robust performance and generalization of unseen data. Observations of minor overfitting were noted, with training accuracy slightly exceeding test accuracy; however, these differences do not significantly detract from the model's effectiveness. The results demonstrate that the KNN algorithm is a promising method for estimating missing well logs, effectively enhancing reservoir characterization workflows in data-limited scenarios.

Introduction

Well logs play a pivotal role in subsurface exploration and reservoir characterization, providing critical data on lithology, porosity, permeability, and other essential reservoir properties. Missing or incomplete well logs pose a significant challenge, potentially leading to inaccurate reservoir models, flawed resource estimates, and increased financial risk in hydrocarbon exploration and development. Incomplete well logs can occur due to tool malfunctions, missing data in legacy wells, or economic constraints that limit the number of well measurements taken. Therefore, developing robust prediction techniques for missing well log data is essential for filling these gaps and enhancing reservoir evaluation.

In recent years, machine learning and artificial intelligence techniques have emerged as effective tools for predicting missing well logs, significantly enhancing prediction reliability and accuracy. For instance, Meng et al. (2024) introduced a generative model based on the conditional denoising diffusion probabilistic model (CDDPM) to impute missing components in well logs. Similarly, Rahmati et al. (2024) integrated Artificial Neural Networks (ANN) with optimization techniques like Genetic Algorithms (GA), Particle Swarm Optimization (PSO), and Imperialist Competitive Algorithms (ICA) to predict density logs, with the GA-ANN model outperforming other approaches. Additionally, Alward et al. (2023) applied a machine learning algorithm incorporating cross-entropy clustering (CEC), Gaussian mixture model (GMM), and Hidden Markov Model (HMM) to predict the same set of zones in new wells requiring interpretation and forecast output curves. This approach enhances the accuracy and efficiency of zonation interpretation and prediction. Furthermore, Qiao et al. (2022) explored a hybrid kernel extreme learning machine optimized through Bayesian methods for addressing missing log challenges. Wu et al. (2021) proposed a hybrid approach combining convolutional neural networks (CNNs) and long short-term memory (LSTM) neural networks to extract spatial and temporal features from well-logging data. They further utilized the particle swarm optimization (PSO) algorithm to optimize hyperparameters of the CNN-LSTM architecture, achieving improved prediction of logging curves. Moreover, Pham et al. (2020) developed a deep learning approach that estimates missing sonic logs using bidirectional recurrent neural networks (BRNN) integrated with convolutional long short-term memory (ConvLSTM) blocks and fully connected neural networks (FCNNs). Additionally, Zhang et al. (2018) utilized recurrent neural networks (RNNs) to generate

synthetic well logs; however, they failed to evaluate the uncertainty in their predictions. Lastly, Salehi et al. (2017) employed artificial neural networks to predict density and resistivity based on conventional wireline logs.

K-Nearest Neighbors (KNN) has been widely utilized in various disciplines, particularly in well logs and geophysics(Prajapati et al., 2024; Barbosa et al., 2022; Gómez et al., 2022; Wu et al., 2018). In this study, KNN regression was chosen over other machine learning methods like Random Forest, Support Vector Machine (SVM), and Decision Trees due to its non-parametric nature, which allows it to model complex, non-linear relationships in multidimensional datasets without assuming an underlying functional form (Srisuradetchai & Suksrikran, 2024; Pan et al., 2015). Additionally, KNN does not require a training phase, making it ideal for real-time tasks.

While methods like Random Forest offer advantages such as uncertainty quantification and feature importance ranking (Feng et al., 2021), they often require significant computational resources, extensive hyperparameter tuning, and larger datasets for optimal performance. These demands can limit their practicality in real-time applications or when working with datasets that have limited observations. In contrast, KNN's simplicity and non-parametric nature make it a computationally efficient and flexible alternative for subsurface data prediction.

Kim and Cho (2024) applied KNN collaborative filtering to impute missing well-log data by identifying similarities between logs, focusing on relationships rather than predicting continuous values. In contrast, KNN regression predicts continuous outcomes by averaging neighboring data points, making it more suitable for missing well-log prediction. Unlike collaborative filtering, which is data-dependent and struggles with sparse datasets (Grčar et al., 2006), KNN regression operates without a training phase or assumptions about data distribution (Goyal et al., 2014), making it a simple, flexible, and effective method for handling missing well log data.

In our research, we propose a novel and easily applicable method to predict missing well logs, specifically Gamma Ray (GR) and Delta T (DT) logs, using the KNN regression algorithm. The workflow for this prediction process, as illustrated in Figure 1, encompasses key steps, including data collection, preprocessing, feature selection, and final model prediction.

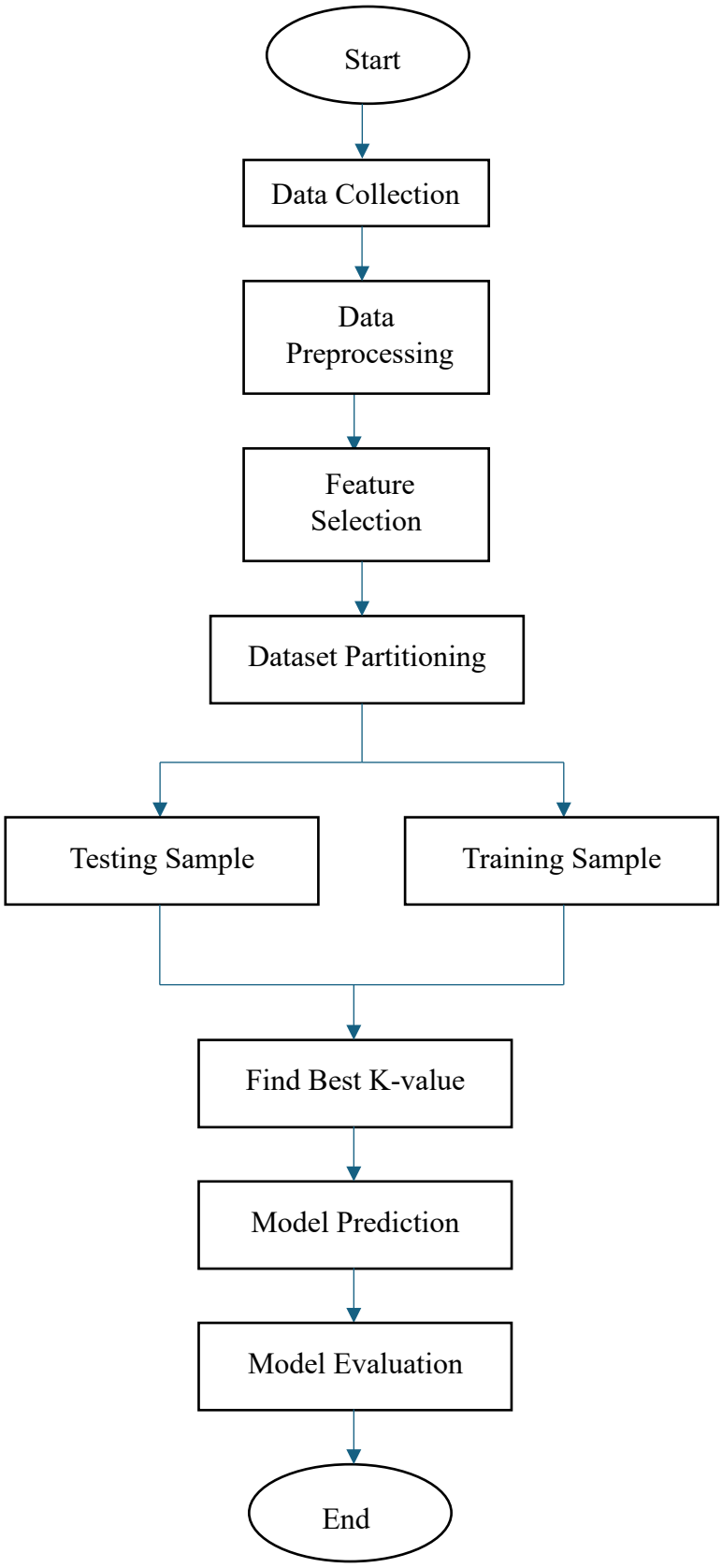

Figure 1: Workflow of the Prediction Process

2. Data and Methods

2.1. Dataset and Preprocessing

The dataset employed in this study was obtained from the University of Kansas and is available via this link. Five wells were selected for analysis: wells 1054310680, 1054310699, and 1054797704 were utilized for predictive modeling of the DT log, whereas wells 1054146917 and 1054357764 were specifically chosen to model GR log.

Figures 2 through 6 illustrate the petrophysical log variables for the five wells (1054310680, 1054310699, 1054797704, 1054146917, and 1054357764) in the studied interval. These variables and their respective units are as follows: Total Bulk Hydrocarbon Volume (TBHV) and Apparent Bulk Hydrocarbon Volume (ABHV) in ft^3; Gamma Ray (GR) in GAPI; Laterolog Resistivity (RILD), Induction Resistivity (RILM), Lateral Log Resistivity (RLL3), and Resistivity at Shallow Depth (RXORT) in Ω-m; Conductivity (CILD, CILM, CLL3) in MMHO/M; Spontaneous Potential (SP) in mV; Caliper (DCAL) in inches; Density Porosity (DPOR), Core Porosity (CNPOR), and Secondary Porosity (SPOR) in PU; Photoelectric Effect (PE) as unitless; Bulk Density (RHOB) and Core Density (RHOC) in g/cc; Microresistivity (MEL15 and MEL20) in Ω-m; Delta T (DT) in μs/ft; Microcaliper (MELCAL) in inches; and Inter-Train Time (ITT) in msec. Rows containing missing values were removed to ensure data quality and integrity across all analyzed wells using a complete-case analysis approach. This ensured that only complete and reliable data points were retained for analysis, minimizing the risk of introducing biases or inaccuracies during model training.

The statistical parameters for the five selected wells are presented in Tables 1 to 5. Well 1054310680 contains 3,409 data points (Table 1), while well 1054310699 contains 2,418 data points (Table 2). Additionally, well 1054797704 also contains 2,645 data points (Table 3), well 1054146917 contains 2,018 data points (Table 4), and well 1054357764 contains 4,232 data points (Table 5). All these wells are included in the analysis.

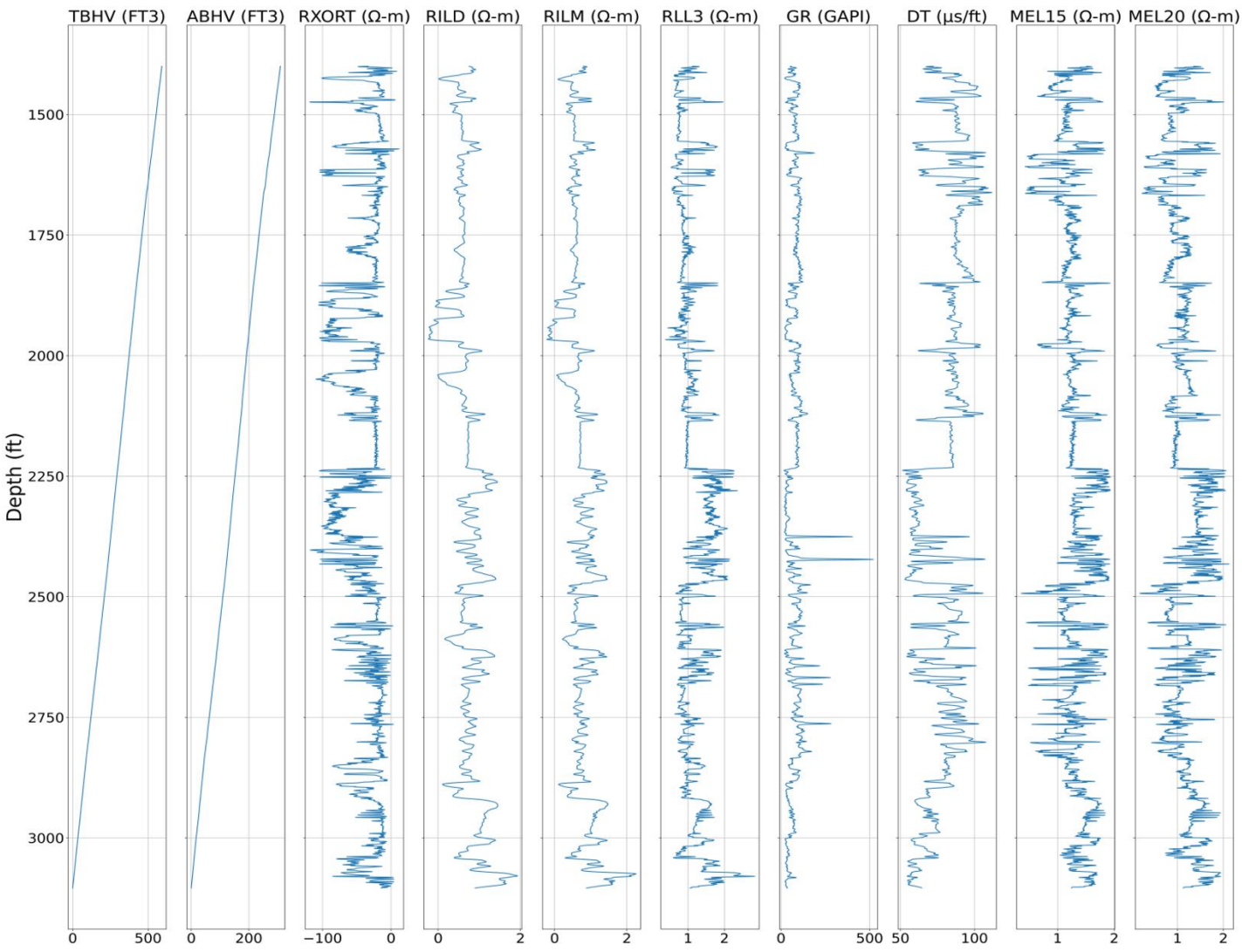

Figure 2: Well logging graph of the Well 1054310680

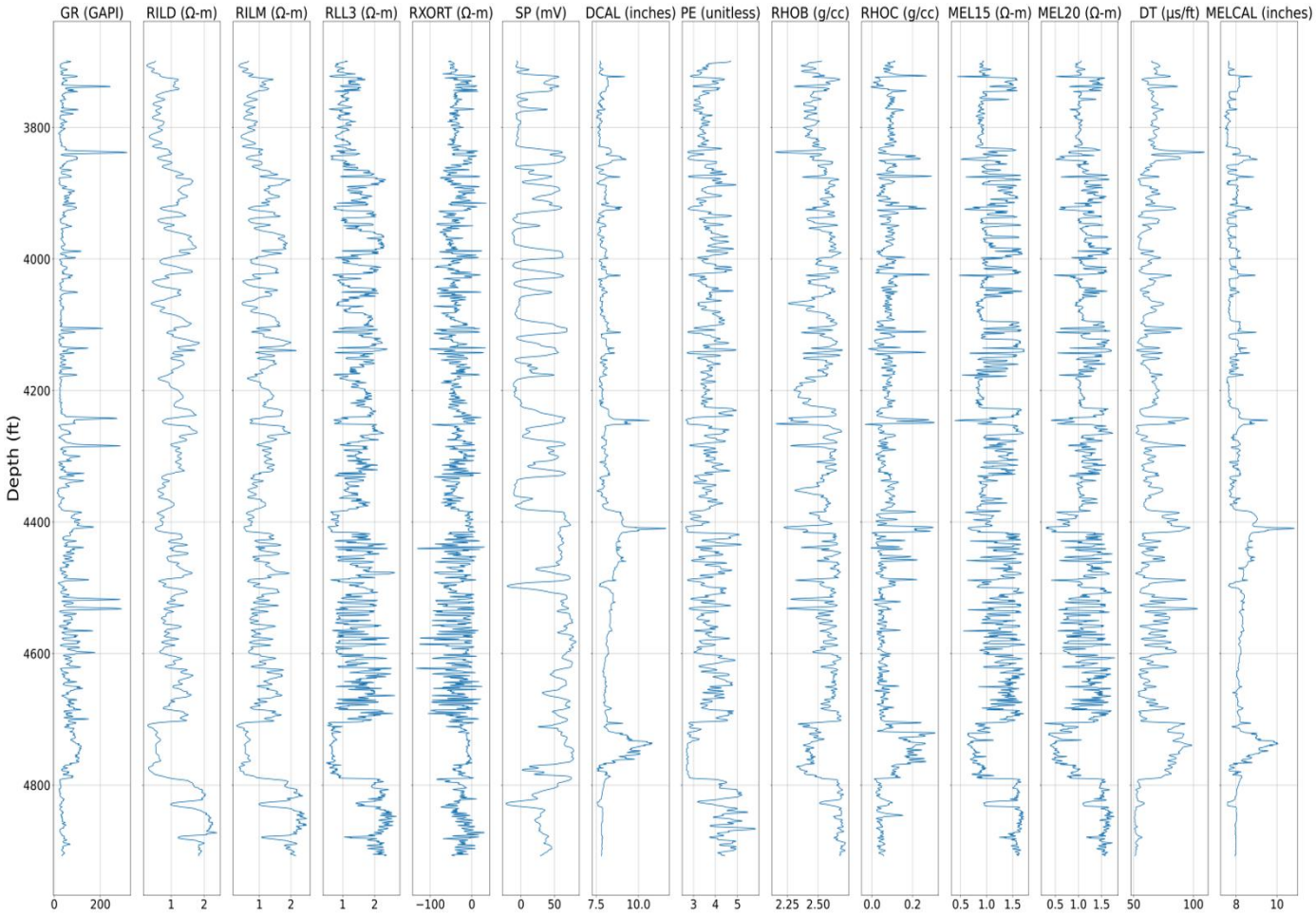

Figure 3: Well logging graph of the Well 1054310699

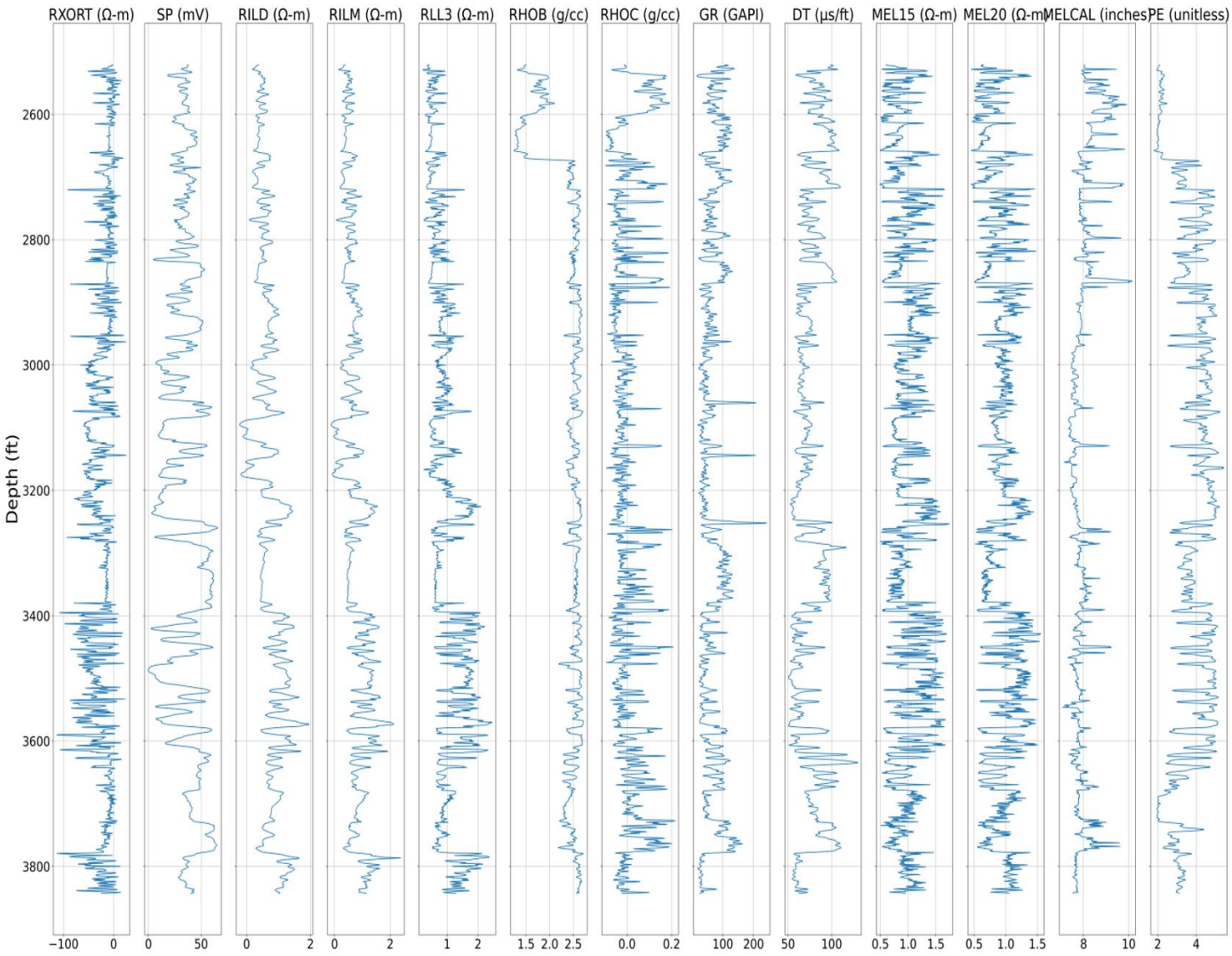

Figure 4: Well logging graph of the Well 1054797704

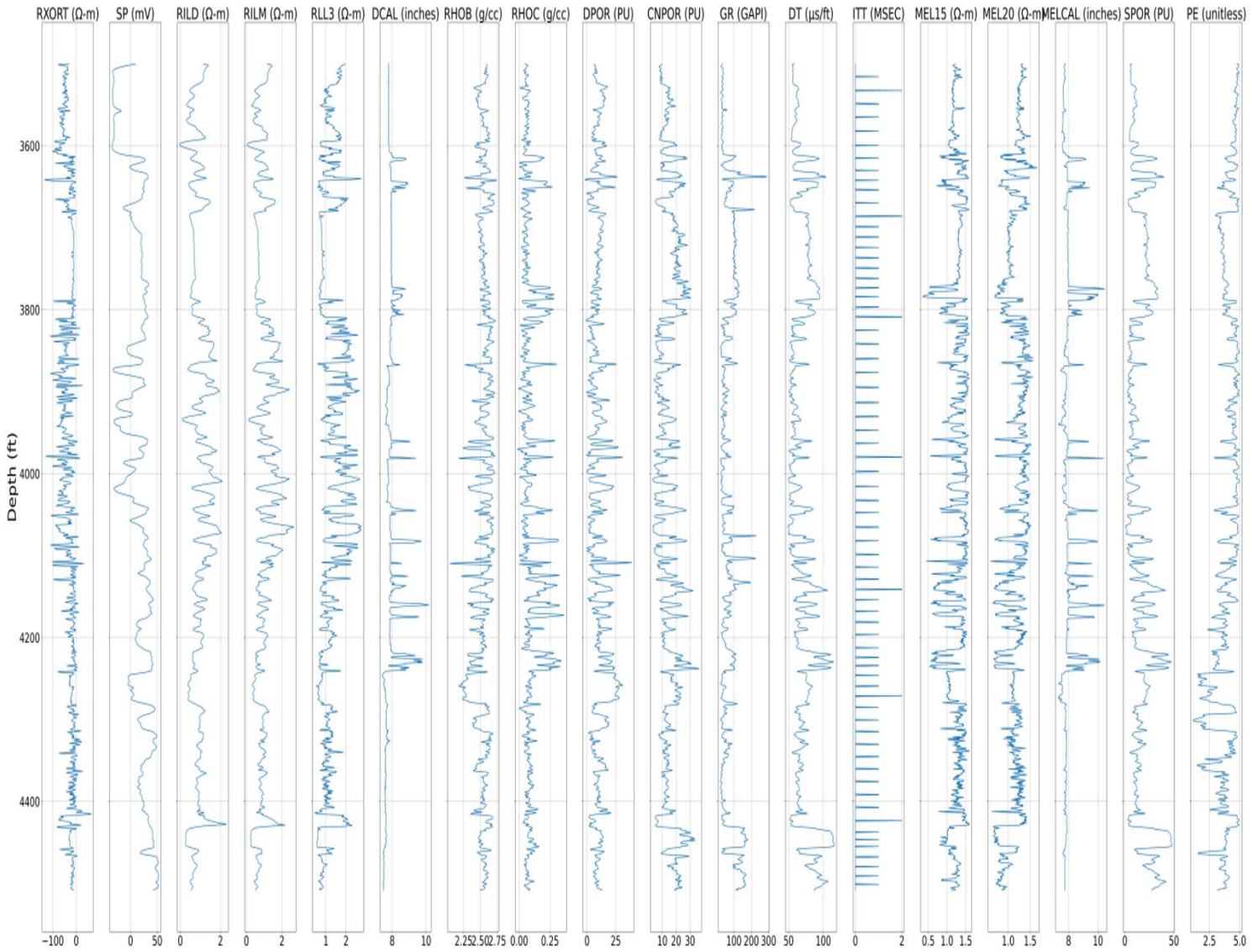

Figure 5: Well logging graph of the Well 1054146917

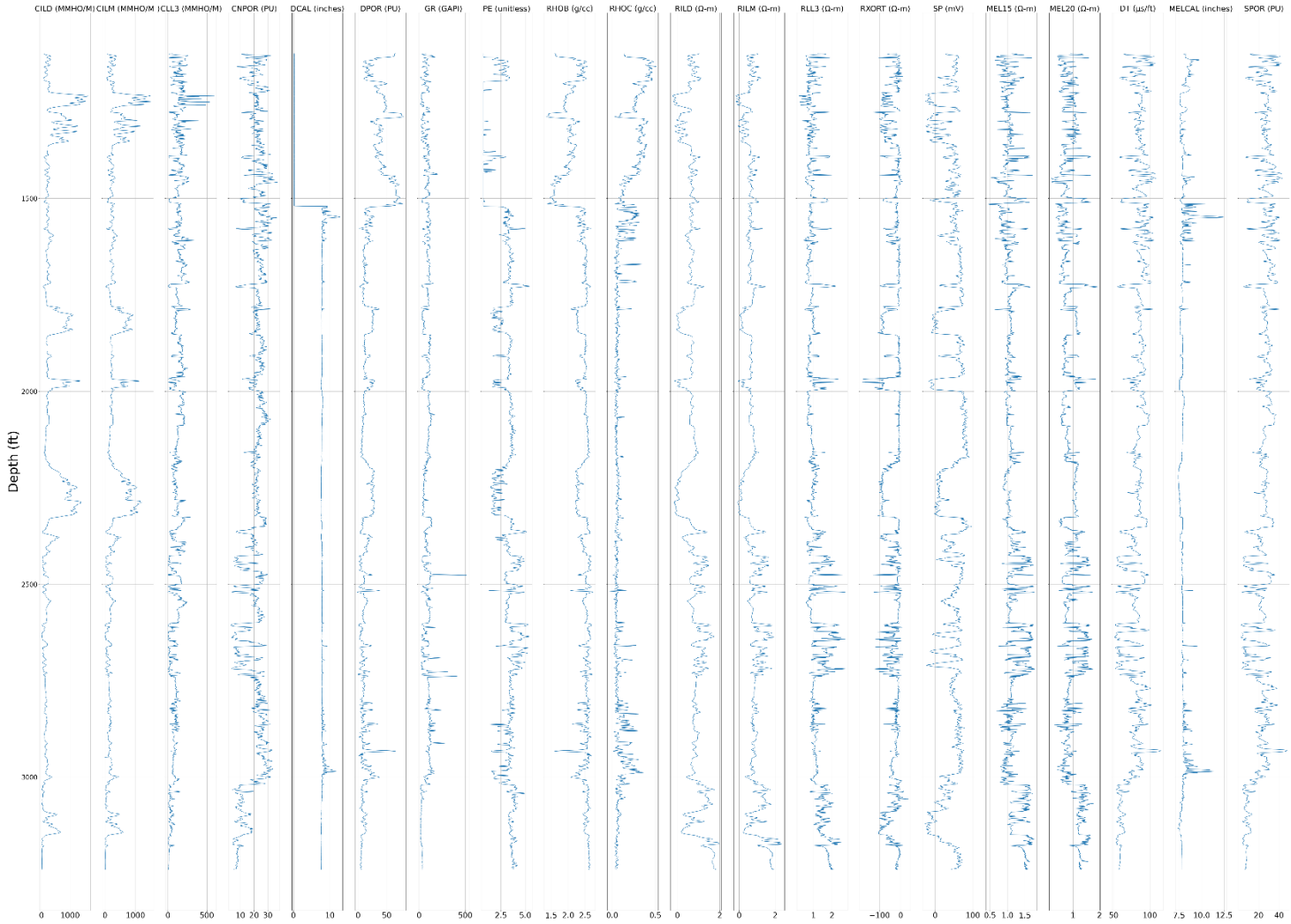

Figure 6: Well logging graph of the Well 1054357764

	TBHV	ABHV	RXORT	RILD	RILM	RLL3	GR	DT	MEL15	MEL20
count	3409.0	3409.0	3409.0	3409.0	3409.0	3409.0	3409.0	3409.0	3409.0	3409.0
mean	291.530846	150.879273	-36.330953	6.675208	7.136873	19.769958	74.716949	79.528714	22.982292	18.621075
std	168.437966	87.268945	26.366208	7.105292	10.93411	30.025319	36.455734	13.285295	15.214074	17.093753
min	0.158700	0.076200	-118.55130	0.57880	0.613900	2.420100	17.59780	51.51100	2.270400	1.507400
25%	146.81830	76.450900	-51.670300	3.60340	3.495600	6.896500	45.72280	67.56450	14.34270	7.550700
50%	292.42360	151.77120	-23.666600	4.48300	4.455100	9.246800	77.64370	83.74430	18.09970	13.27740
75%	432.68490	221.74990	-17.792100	6.89540	6.942300	21.66270	97.61820	88.25140	25.50860	22.87530
max	591.1821	309.96210	11.621100	85.1740	181.7632	674.9022	520.4186	111.7154	85.61880	132.6278

165

166 *Table 1. Statistical parameters of the Well 1054310680.*

167

	GR	RILD	RILM	RLL3	RXORT	SP	DCAL	PE	RHOB	RHOC	MEL15	MEL20	DT	MELCAL
count	2418.0	2418.0	2418.0	2418.0	2418.0	24180	2418.0	2418.0	2418.0	2418.0	2418.0	2418.0	2418.0	2418.00
mean	53.619885	20.822965	27.148209	53.856124	-33.003904	32.935675	8.144792	3.721710	2.544099	0.078830	19.553072	18.174411	65.504488	8.067194
std	35.061367	28.365211	40.784066	63.687986	24.219610	29.484940	0.493014	0.584979	0.103241	0.050819	13.402699	11.998157	10.464084	0.415852
min	12.471700	1.833300	1.887800	3.084200	-133.720800	-22.411500	7.487700	2.638600	2.152400	-0.033700	2.449400	1.875300	50.674500	7.411000
25%	30.440350	5.542650	6.022150	9.859625	-48.354525	1.444350	7.837250	3.340725	2.469550	0.043800	8.217950	10.062375	57.465375	7.718850
50%	42.192850	11.451950	12.785800	29.349650	-33.989100	36.862000	8.028100	3.662350	2.564500	0.068950	13.263600	13.202900	63.764900	8.038700
75%	67.696550	21.872350	27.649575	75.991000	-14.466975	60.353100	8.231850	4.134375	2.627325	0.096800	31.124025	26.061375	70.044650	8.200750
max	316.16450	243.42780	315.74070	484.727800	34.57170	82.19810	11.59920	5.818900	2.72110	0.311200	54.435100	60.88480	109.2734	10.8480

168 *Table2. Statistical parameters of the Well 1054310699*

169

170

171

	RXORT	SP	RILD	RILM	RLL3	RHOB	RHOC	GR	DT	MEL15	MEL20	MELCAL	PE
count	2645.0	2645.0	2645.00	2645.0	2645.0	2645.0	2645.0	2645.0	2645.0	2645.0	2645.0	2645.0	2645.0
mean	-22.217955	35.572337	7.087769	8.123798	17.667461	2.431657	0.000970	63.619059	75.542748	11.918631	9.598402	7.928483	3.724150
std	21.366533	15.536459	7.935506	12.234151	30.294793	0.330134	0.061827	32.057168	15.557110	8.668763	5.385613	0.444585	0.974784
min	-113.382800	-0.216000	0.606200	0.754300	1.604100	1.243700	-0.097000	15.205500	50.302900	3.097400	2.841000	7.076400	1.815200
25%	-36.562000	24.977800	2.770400	2.850600	3.991800	2.425500	-0.041400	37.769300	62.729500	6.119100	5.390500	7.662100	3.001900
50%	-14.865000	36.379200	4.271500	4.361400	6.175000	2.540700	-0.018300	53.799900	72.489600	8.582800	8.330500	7.813500	3.837600
75%	-7.412200	47.328800	7.715000	8.242800	13.460400	2.619300	0.023900	87.877700	87.823900	14.849900	12.059700	8.034600	4.595100
max	25.245000	65.830100	91.810000	238.250100	286.950700	2.720000	0.215400	241.847300	130.042400	55.195400	35.561700	10.151800	5.427100

Table3. Statistical parameters of the Well 1054797704.

	RXORT	SP	RILD	RILM	RLL3	DCAL	RHOB	RHOC	DPOR	CNPOR	GR	DT	ITT	MEL15	MEL20	MELCAL	SPOR	PE
count	2018.0	2018.0	2018.0	2018.0	2018.0	2018.0	2018.0	2018.0	2018.0	2018.0	2018.0	2018.0	2018.0	2018.0	2018.0	2018.	2018	2018
mean	-29.965611	14.320710	13.321736	18.156369	43.817104	7.870437	2.542324	0.085456	9.811414	14.476617	63.911609	68.999756	0.056987	20.365750	16.212603	7.926585	15.134199	4.024079
std	24.965007	23.346003	17.200970	36.062706	79.737782	0.324729	0.103518	0.062138	6.053487	6.562245	40.212291	14.718520	0.254310	8.801552	6.900999	0.404957	10.409138	0.780107
min	-135.484900	-34.481400	0.924400	1.107900	2.814500	7.428800	2.047100	-0.013700	-1.696700	2.973200	20.456700	48.832600	0.000000	2.273300	3.946200	7.290400	0.871700	1.159500
25%	-46.513900	1.287200	4.366700	4.146325	6.602425	7.673200	2.496425	0.049425	5.501975	9.349225	32.891925	57.131625	0.000000	13.787200	10.621625	7.754800	6.740900	3.629500
50%	-22.487800	20.748150	7.190800	6.917150	12.578100	7.838300	2.555000	0.068600	9.080650	13.434000	46.341300	64.443000	0.000000	19.783000	16.320050	7.857050	11.911600	4.108850
75%	-11.540875	30.508250	14.014825	15.082600	41.262600	7.942250	2.615900	0.093600	12.491250	19.618350	93.159350	78.460400	0.000000	27.474025	21.444500	7.945225	21.824925	4.692500
max	63.36740	52.4452	192.890	463.6503	577.4621	10.1594	2.7390	0.3642	38.7668	36.7191	289.373	115.8316	2.0000	39.9105	45.3835	10.450000	48.2543	5.0003

Table4. Statistical parameters of the Well 1054146917

.

	CILD	CILM	CLL3	CNPOR	DCAL	DPOR	GR	PE	RHOB	RHOC
count	4232.0	4232.0	4232.00	4232.0	4232.0	4232.0	4232.0	4232.0	4232.0	4232.0
mean	293.285003	268.023889	112.988119	20.870827	6.452647	18.376862	82.846572	2.894391	2.395756	0.115481
std	295.241424	238.936506	65.057653	6.675758	2.988803	15.211531	39.523313	1.120464	0.260117	0.106345
min	10.834300	0.000	1.9053	3.236800	0.2324	-1.043300	15.44320	0.70	1.36160	-0.02800
25%	136.628525	137.805200	66.974650	18.456925	7.667975	8.463475	48.405300	2.280575	2.287475	0.051500
50%	197.504050	203.520400	112.579600	22.407550	7.794750	11.974500	91.063000	3.312450	2.505250	0.065300
75%	273.876250	279.016125	157.996725	25.238925	7.850750	24.707400	110.836325	3.562550	2.565300	0.128400
max	1624.782300	1510.19650	594.339100	36.93080	12.90600	78.85560	514.05580	5.46520	2.727800	0.50810

	RILD	RILM	RLL3	RXORT	SP	MEL15	MEL20	DT	MELCAL	SPOR
count	4232.0	4232.0	4232.0	4232.0	4232.0	4232.0	4232.0	4232.0	4232.0	4232.0
mean	8.078386	9.210663	20.042775	-32.015903	44.654253	15.429559	10.857855	81.016635	7.932830	23.632700
std	10.541830	15.676824	35.918322	31.040656	28.216984	10.183541	9.075430	12.626940	0.376942	8.929943
min	0.615500	0.66220	1.68250	-182.5404	-25.8694	2.8475	1.558300	51.273100	7.350600	2.5977
25%	3.651250	3.583975	6.329225	-52.068300	23.514050	9.791250	4.899375	75.236150	7.795300	19.544650
50%	5.063200	4.913550	8.882600	-17.168600	53.700900	11.821050	6.958500	84.086700	7.885850	25.803900
75%	7.319125	7.247825	14.931000	-8.869125	66.476400	14.955675	13.545925	89.220125	7.942950	29.434300
max	92.299400	245.8668	524.8573	36.8242	96.3551	60.2055	85.1321	114.9641	12.4807	47.6408

Table 5. Statistical parameters of Well 1054357764.

2.2 Correlation Analysis

Pearson's correlation is widely used to assess how strongly two numerical variables are related. It provides a numerical value quantifying the linear relationship between two variables (Wilcox, 2003). As a parametric method, it relies on the mean parameter of the data, making it particularly valid for normally distributed datasets (Nettleton, 2014). The coefficient calculates a score ranging from -1 to +1, where 0 indicates no correlation, +1 signifies total positive correlation, and -1 indicates total negative correlation (Kumar & Reinartz, 2014). According to Turney (2022), a Pearson correlation coefficient greater than 0.5 indicates a strong correlation, between 0.3 and 0.5 suggests a moderate correlation, and between 0 and 0.3 reflects a weak correlation. Negative values follow the same pattern. In this study, to achieve more accurate predictions, we will incorporate variables with moderate to strong correlations into the predictive model, specifically those with Pearson correlation coefficients greater than 0.3 or less than -0.3. The Pearson correlation coefficient for each well was calculated between the target variables (DT or GR) and other log variables. Variables that exhibited correlations above 0.3 or below -0.3 were selected as relevant features for the model. This approach ensures the inclusion of only the most significant variables, thereby enhancing the accuracy and robustness of the predictive model. The formula for calculating the Pearson correlation coefficient for a sample is:

$$r = \frac{n(\sum xy) - (\sum x)(\sum y)}{\sqrt{[n\sum x^2 - (\sum x)^2][n\sum y^2 - (\sum y)^2]}} \quad (1)$$

Where:

- n is the number of pairs of scores,
- x and y are the individual sample points,
- $\sum xy$ is the sum of the product of paired scores

Figures 7 through 9 present the Pearson correlation coefficients between DT and various other logs for wells 1054310680, 1054310699, and 1054797704, respectively. For well 1054310680, the selected logs exhibiting moderate to strong correlations with DT include TBHV, ABHV, RXORT, RILD, RILM, RLL3, GR, DT, MEL15, and MEL20. In well 1054310699, the logs GR, RILM, RLL3, RXORT, SP, DCAL, RHOB, RHOC, MEL15, MEL20, and MEL20 displayed moderate to strong correlations with DT. Similarly, for well 1054797704, RXORT, SP,

RILD, RILM, RLL3, RHOB, RHOC, GR, MEL15, MEL20, MELCAL, and PE demonstrated moderate to strong correlations with DT.

Figures 10 and 11 illustrate the Pearson correlation coefficients between the GR log and other logs for wells 1054146917 and 1054357764, respectively. For well 1054146917, the logs with moderate to strong correlations with GR include RXORT, SP, RILD, RILM, RLL3, DCAL, RHOC, CNPOR, DT, MEL15, MEL20, MELCAL, SPOR, PE, RHOB, DPOR, and RILM. In well 1054357764, the selected logs showing moderate to strong correlations with GR are CILD, CLL3, CNPOR, RILM, RLL3, RXORT, SP, MEL15, MEL20, DT, MELCAL, and SPOR.

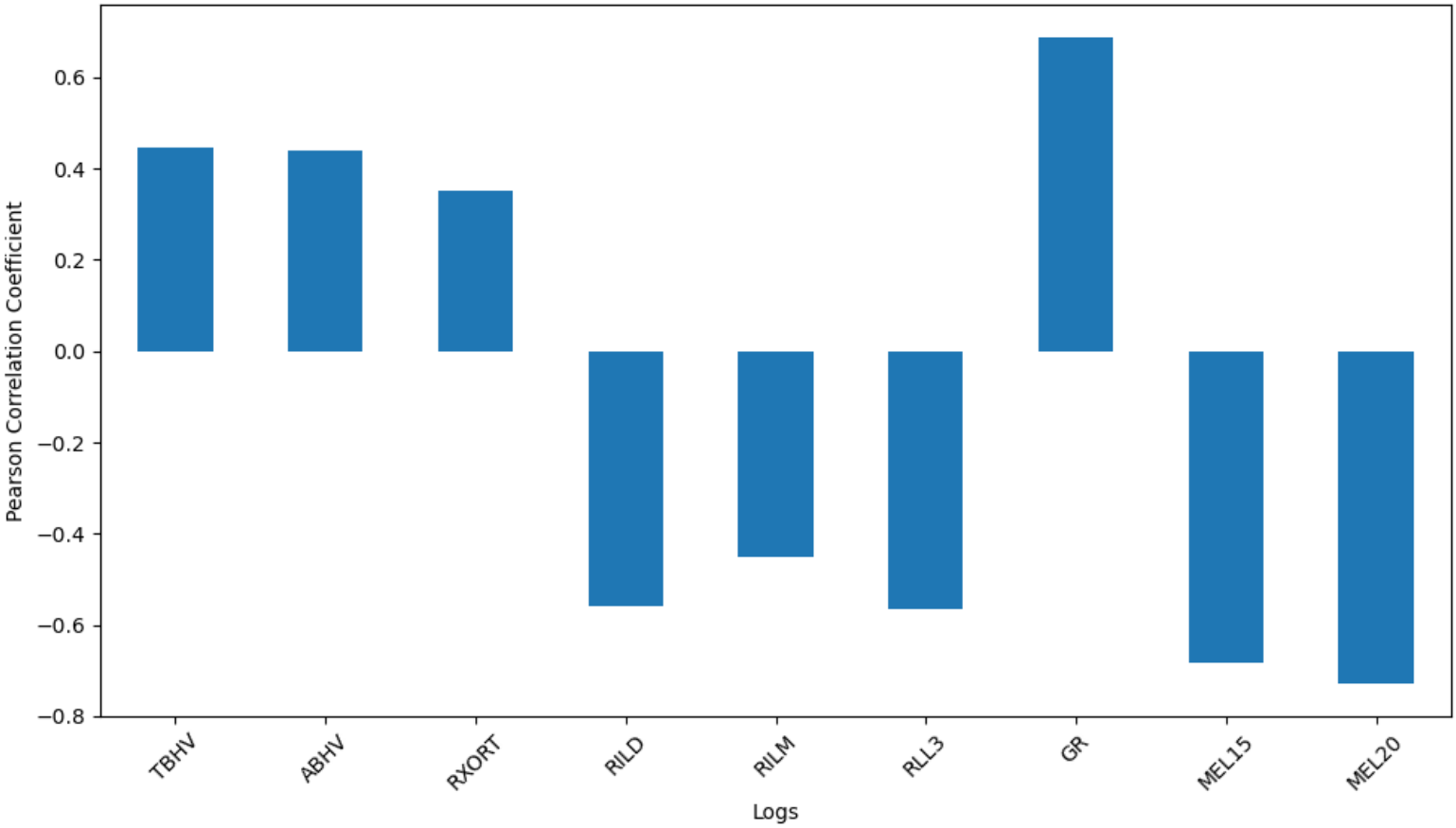

Figure 7: Pearson Correlation between DT log and other Logs for the well 1054310680

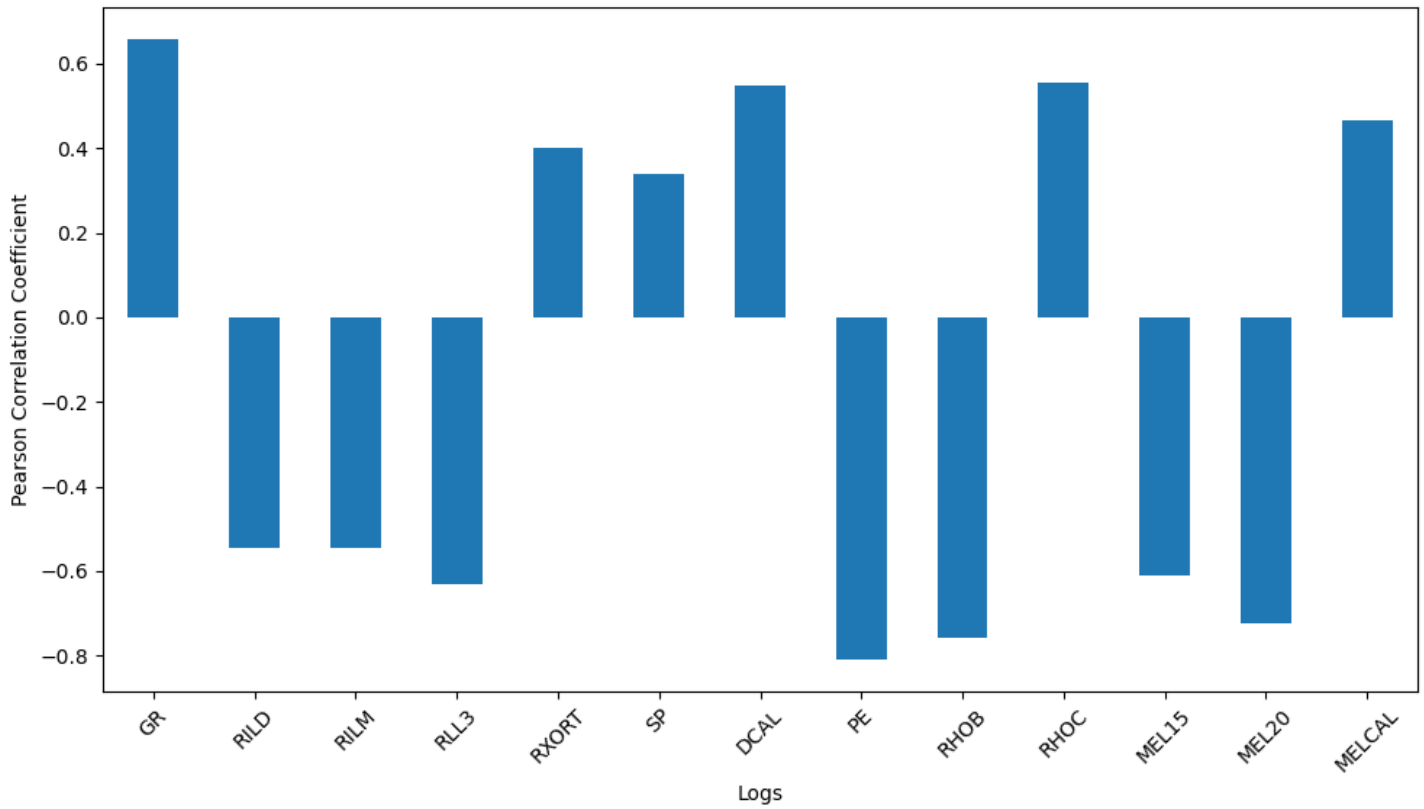

Figure 8: Pearson Correlation between DT log and other Logs for the well 1054310699

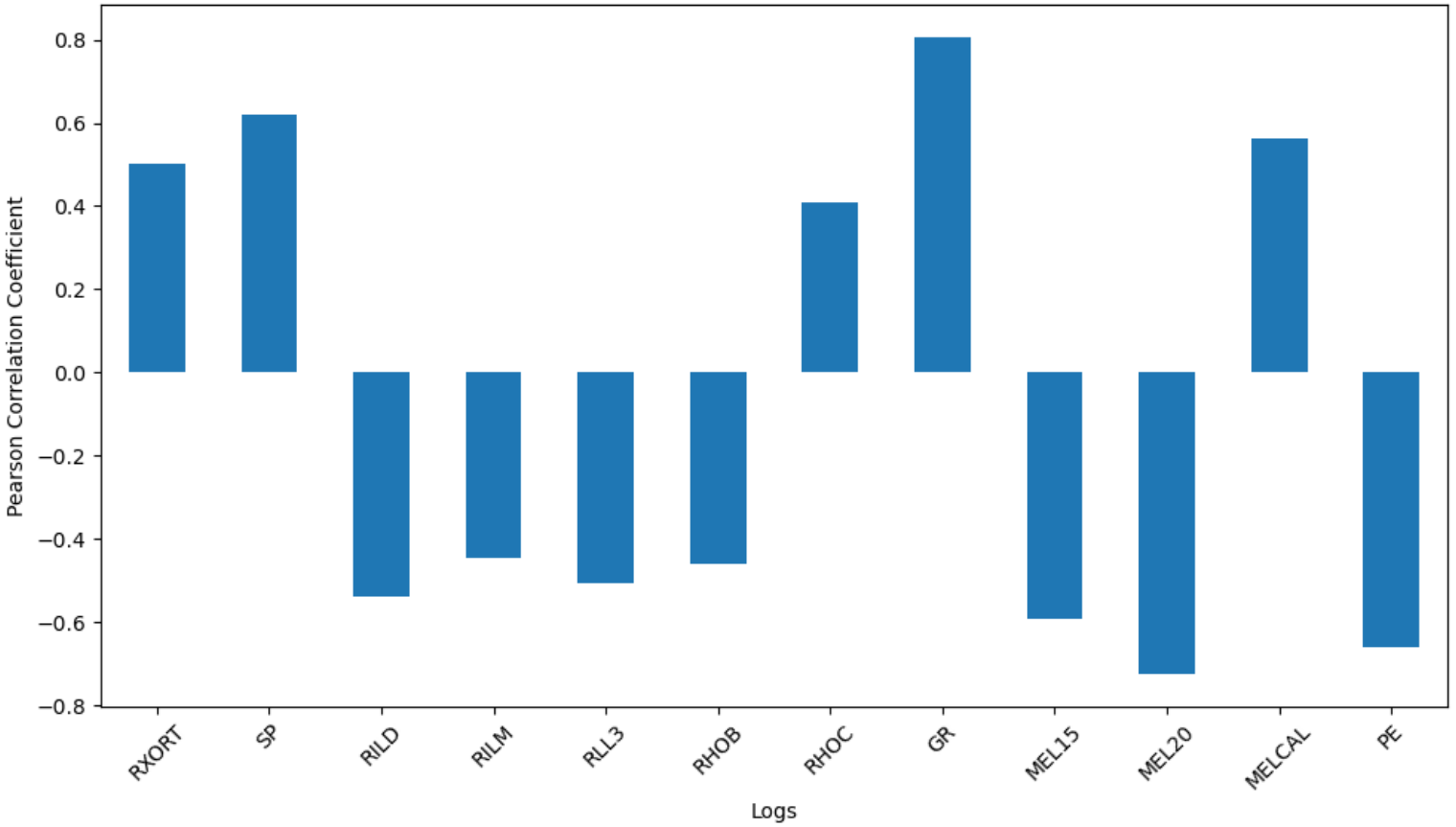

Figure 9: Pearson Correlation between DT log and other Logs for the well 1054797704

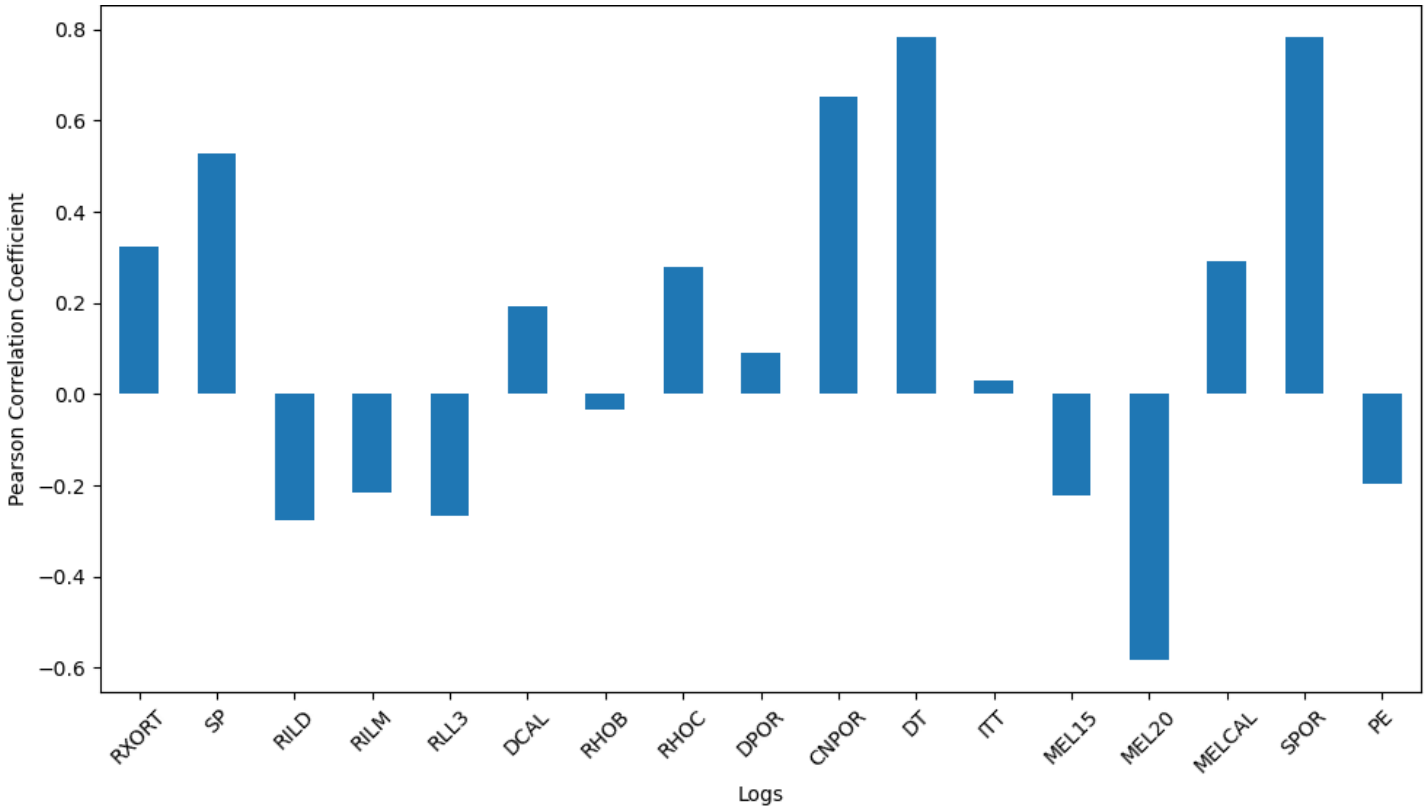

Figure 10: Pearson Correlation between GR log and other Logs for the well 1054146917

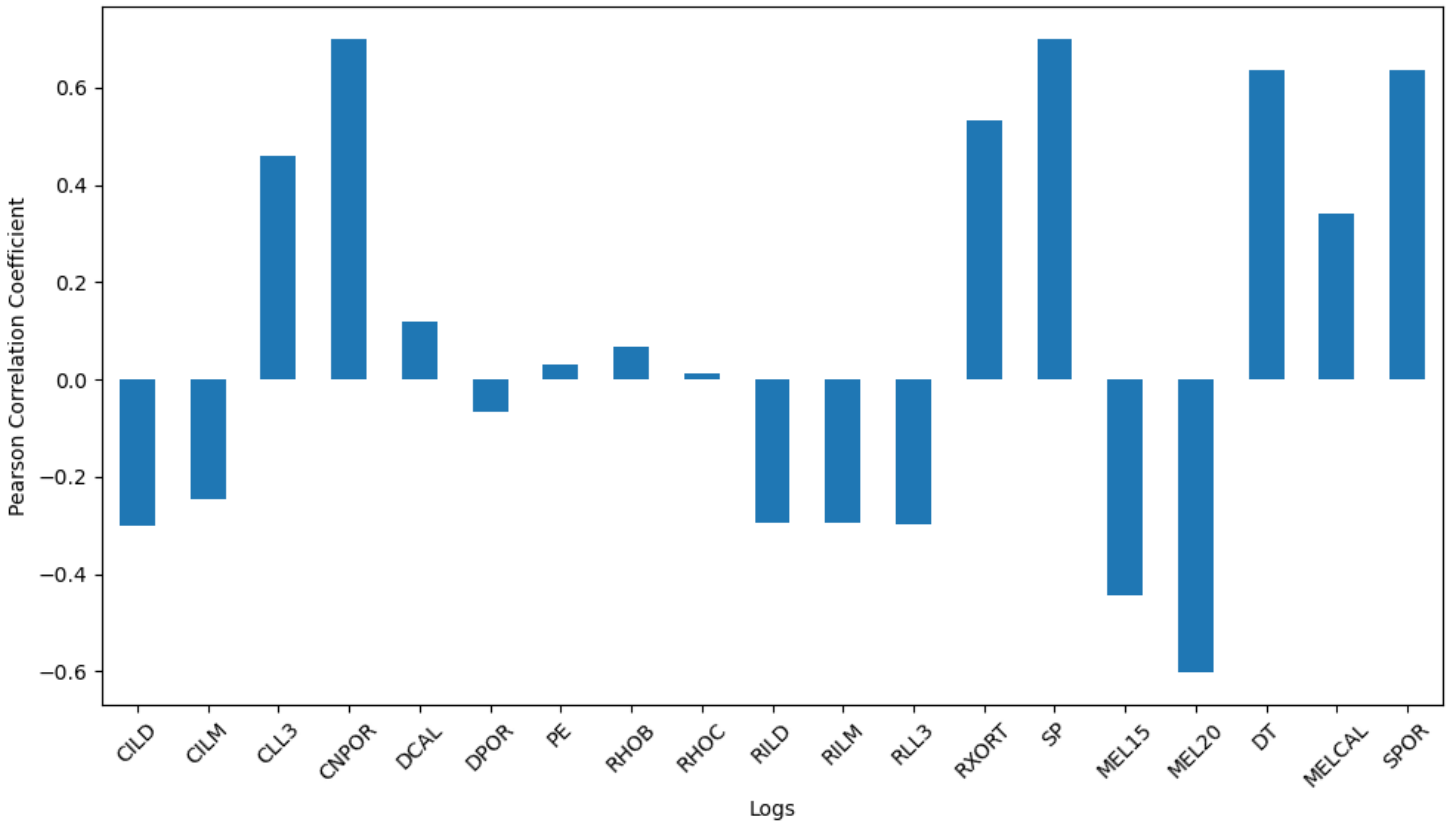

Figure 11: Pearson Correlation between GR log and other Logs for the well 1054357764

2.3 Data Splitting and Validation

The dataset was divided into training and testing sets using a split ratio of 70/30, where 70% of the data was designated for training and 30% for testing. This approach ensures that the model has a substantial amount of data for training while retaining enough for evaluating its performance on unseen examples (Raykar & Saha, 2015). Empirical studies suggest that allocating 20–30% of data for testing and 70–80% for training achieves optimal results in machine learning by reducing overfitting and improving generalization (Gholamy et al., 2018). The 70% training split helps the model learn patterns effectively, especially with smaller datasets, while the 30% testing split ensures reliable and statistically significant performance evaluation. To enhance the reproducibility of the results, a random state of 42 was employed during the splitting process (Shchutskaya, 2021).

The training accuracy and test accuracy were then computed using the coefficient of determination (R^2), which measures how well the model fits both the training and testing data. The R^2 value ranges from 0 to 1, where an R^2 value of 1 indicates a perfect fit to the data, meaning that the model explains all the variability in the response variable. Conversely, an R^2 value of 0 suggests that the model does not explain any variability, indicating a poor fit. This approach allows for a comprehensive evaluation of the model's performance on both known and new data, helping identify any potential overfitting or underfitting issues (Picard & Berk, 1990). The coefficient of determination is defined by the equation(2):

$$R^2 = 1 - \frac{\sum(y_i - \hat{y}_i)^2}{\sum(y_i - \bar{y})^2} \qquad (2)$$

Where:

- y_i are the values observed
- $\hat{y}_i$ are the predicted values
- $\bar{y}$ is the mean of the observed values

the max–min normalization method was employed to address the challenge of diminished pattern recognition in the network resulting from the wide range of input data(Ali, 2022). This technique limits the features, thereby accelerating optimization, eliminating data offsets, and ensuring that each feature contributes equally to the model. By normalizing the dataset to a range of 0 to 1, this scaling is crucial for algorithms like KNN (Henderi, 2021), which rely on distance metrics sensitive to data scale. The expression of the max-min normalization method is as follows:

$$X' = \frac{X - X_{\min}}{X_{\max} - X_{\min}} \qquad (3)$$

Where:

- X is the original value
- X' is the normalized value
- $X_{\min}$ and $X_{\max}$ are the minimum and maximum values of the feature, respectively

2.4 KNN Regression

KNN Regression is a supervised machine learning algorithm. It is a simple, effective, and robust nonlinear regression method (Benedetti,1977). The fundamental concept of KNN regression involves predicting an output value for a given input sample by analyzing a predetermined number (k) of its closest neighbors identified from the training dataset (Mailagaha Kumbure & Luukka, 2021). This method leverages the relationship between input-output pairs to make accurate predictions based on proximity in the feature space. The concept of the KNN regression model has been addressed in various studies, including Song et al. (2017), Hu et al. (2014), Kramer (2011), and Stone (1977). The notion of the KNN regression model can be formally defined as follows.

The first step in KNN regression is to calculate the distance between the new data sample (X) and each sample (X_i) in the training dataset (T). The Euclidean distance is commonly used and is calculated as follows:

Given:

- $X = \{X_1, X_2, \ldots, X_m\}$
- $X_i = \{X_1^i, X_2^i, \ldots, X_m^i\}$

The Euclidean distance is presented by Equation (4):

$$d(X, X_i) = \sqrt{\sum_{j=1}^{m} (x_j - x_{ij})^2} \qquad (4)$$

This equation measures the straight-line distance between the points X and X_i in the (m)-dimensional feature space. Once the distances are calculated, the next step is to identify the (k) nearest neighbors. This involves sorting the distances and selecting the k smallest ones.

The predicted value ($\hat{y}$) for the new sample (X) is the average of the output values Y_i of the nearest neighbors. This can be expressed as Equation (5):

$$\hat{y} = \frac{1}{k} \sum_{i=1}^{k} Y_i \qquad (5)$$

3. Results

3.1 Model Performance

The parameter **k** represents the number of nearest neighbors considered when making a prediction for a data point. The value of K is a critical parameter in the KNN regression model and can significantly affect its performance. Smaller K values tend to make the model more responsive to noise, which can result in overfitting. Conversely, larger K values reduce overfitting but may also diminish the model's precision, as more distant neighbors are considered. The Root Mean Square Error (RMSE) metric was utilized to evaluate performance across different K values. RMSE, computed as Equation (6):

$$\text{RMSE} = \sqrt{\frac{1}{n}\sum_{i=1}^{n}(y_i - \hat{y}_i)^2} \qquad (6)$$

where:

n is the number of observations,

y_i represents the actual value for the i -th observation,

$\hat{y}_i$ represents the predicted value for the i -th observation.

RMSE measures the differences between the predicted and actual values, with higher penalties for larger errors, making it particularly useful for assessing model accuracy. A lower RMSE indicates better model performance. Evaluating RMSE across various K values enables the identification of the optimal K that minimizes error and balances bias and variance. A lower RMSE reflects improved predictive accuracy, with the optimal K effectively reducing variance without increasing bias.

Figures 12 to 16 illustrate the relationship between the number of neighbors and the corresponding RMSE values for KNN model applied to well 1054310680, 1054310699, 1054797704,1054146917 and 1054357764 respectively.

For well 1054310680, the lowest RMSE occurs at k=3, indicating it is the optimal choice for minimizing error, with an RMSE of approximately 3.13 (Figure 12). In the case of well 1054310699, the lowest RMSE occurs at k=2, making it the optimal choice for minimizing error, with an RMSE of approximately 2.01 (Figure 13). For well 1054797704, the lowest RMSE also occurs at k=2, which is the optimal choice for minimizing error, resulting in an RMSE of approximately 3.22 (Figure 14).

For well 1054146917, the optimal choice for minimizing error is at k=3, yielding an RMSE of approximately 11.16 (Figure 15). Lastly, for well 1054357764, the lowest RMSE occurs at k=4, which is the optimal choice for minimizing error, with an RMSE of approximately 9.74 (Figure 16).

The observed trends in the RMSE vs. k graphs highlight the effectiveness of the KNN model in adapting to the unique characteristics of each well through k-tuning, demonstrating the robustness and flexibility of the chosen approach. For each well, the specific optimal k minimizes error while effectively balancing bias and variance, directly aligning with the study's objective to achieve accurate and reliable predictions.

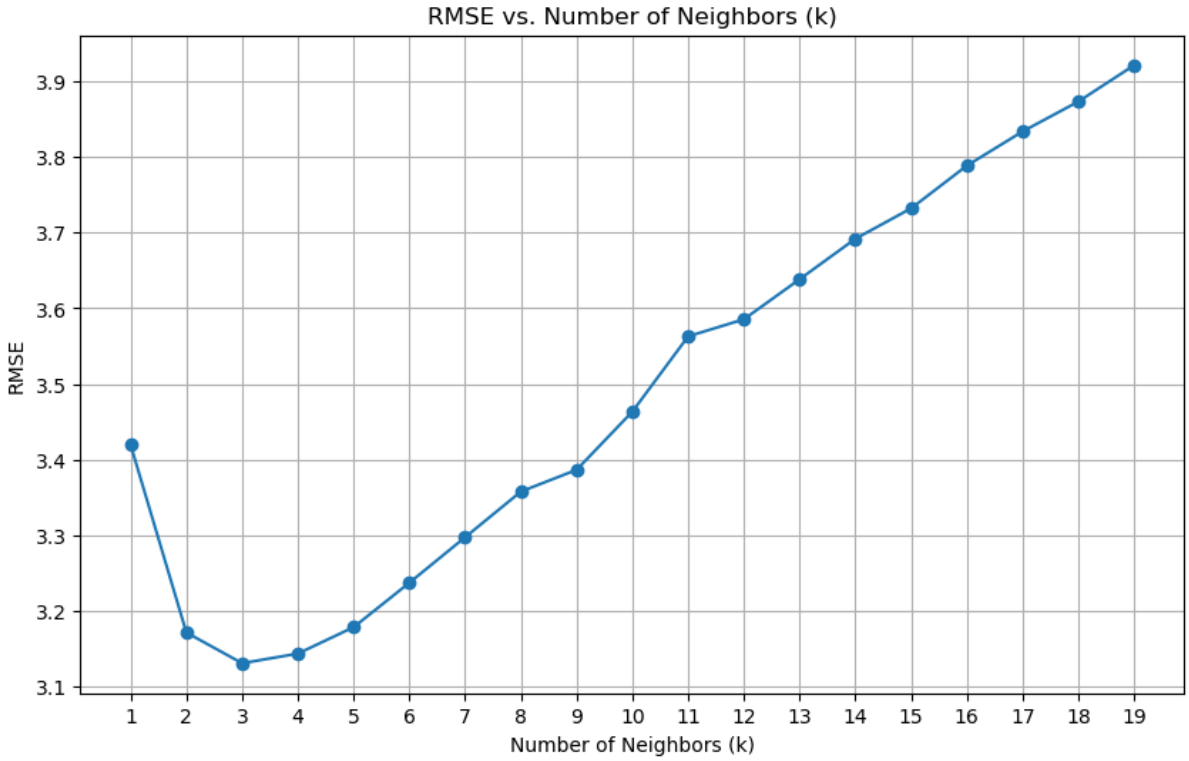

Figure 12: RMSE Values for Different K in KNN Regression for well 1054310680.

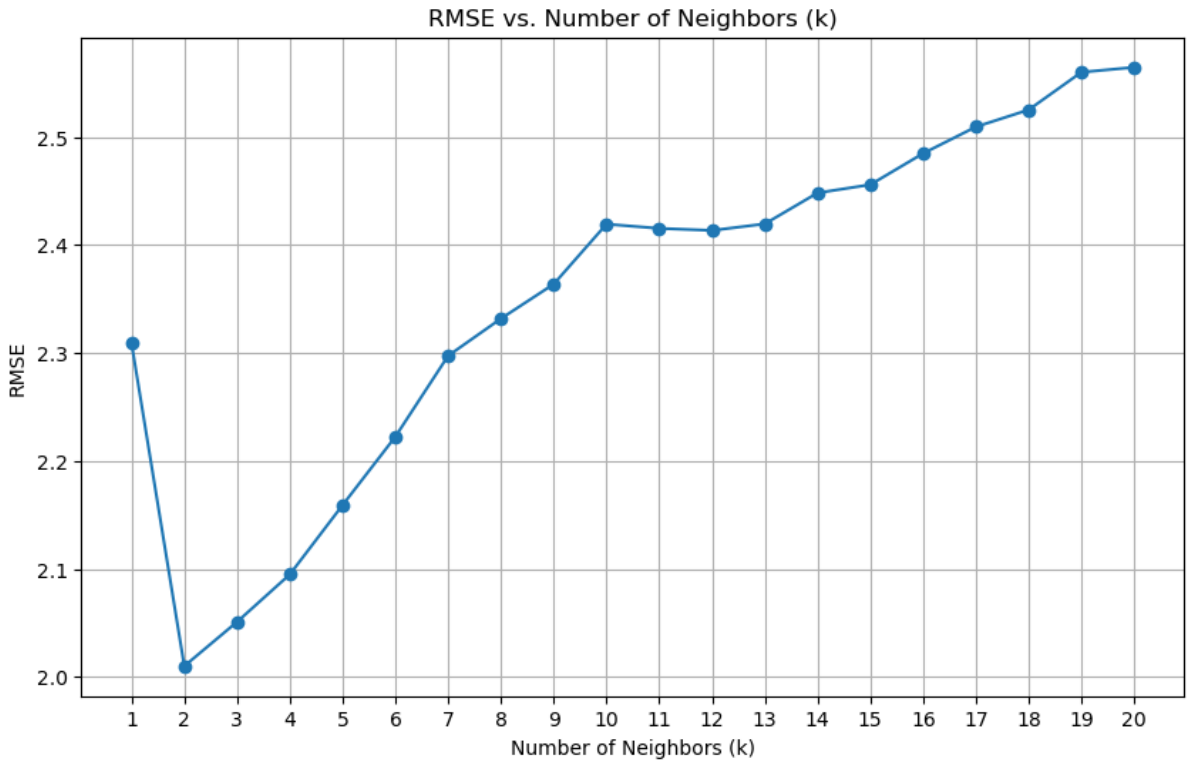

Figure 13: RMSE Values for Different K in KNN Regression for well 1054310699.

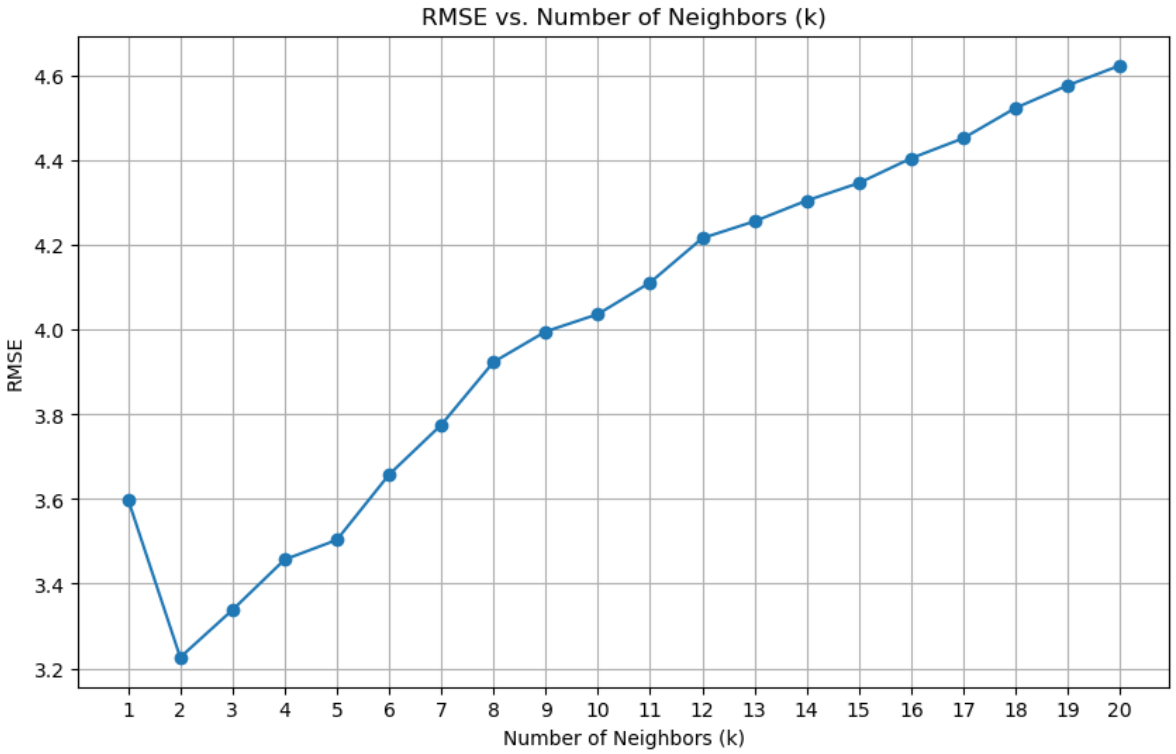

Figure 14: RMSE Values for Different K in KNN Regression for well 1054797704

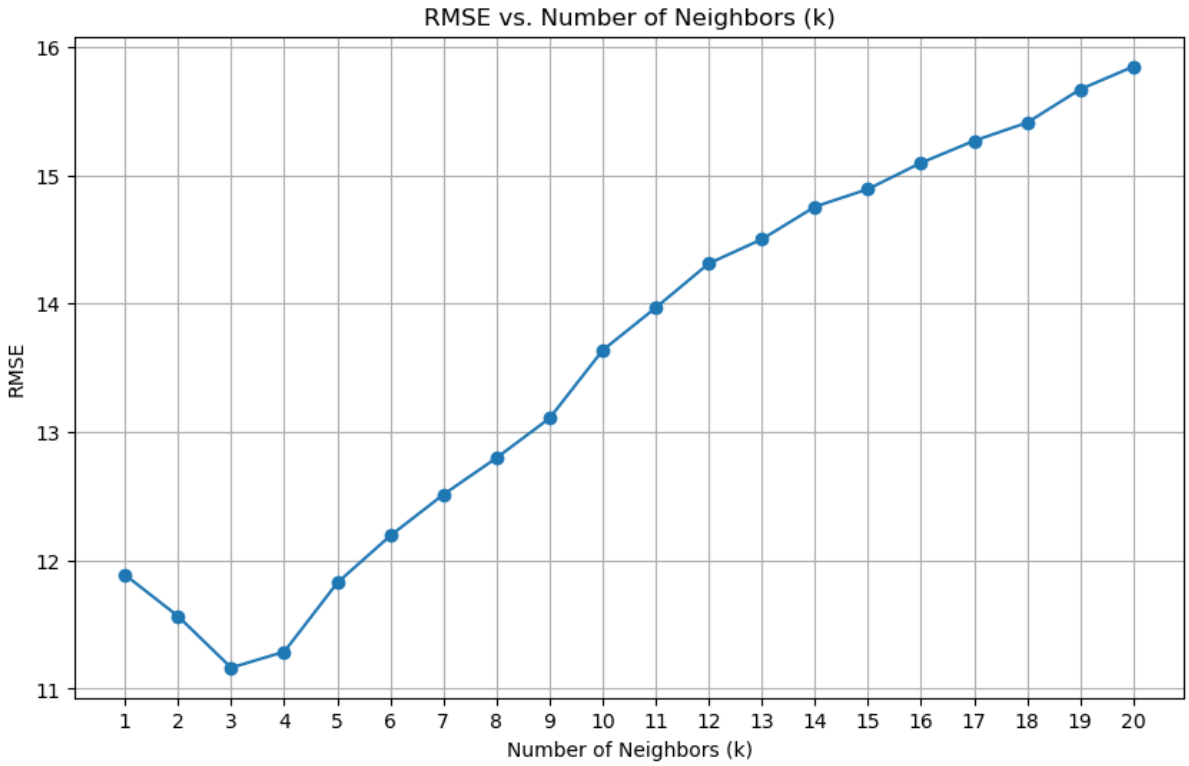

Figure 15: RMSE Values for Different K in KNN Regression for well 1054146917.

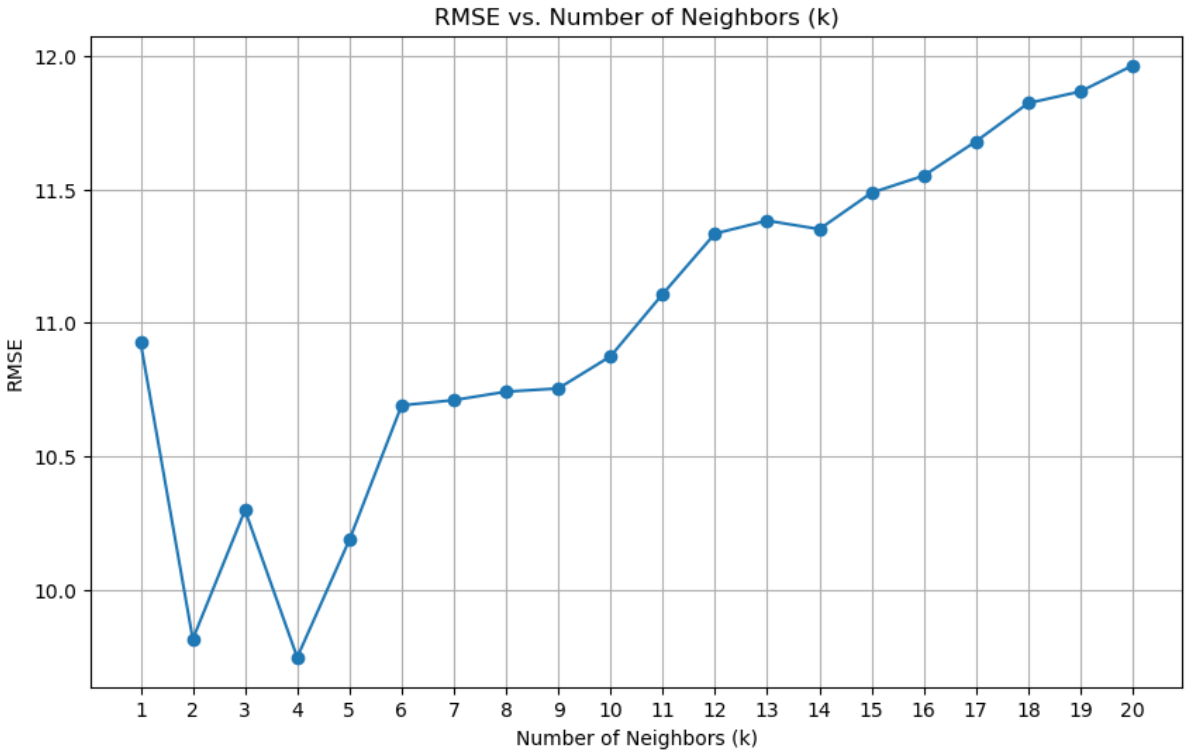

Figure 16: RMSE Values for Different K in KNN Regression for well 1054357764.

3.2 Model Validation

The performance of the KNN model was assessed across five wells and various logs, specifically DT and GR, yielding significant accuracy scores. For the DT log, well 1054310680 achieved a Training Accuracy Score of 0.976 and a Test Accuracy Score of 0.942 (Figure 17). In Well 1054310699, the model attained a Training Accuracy Score of 0.988 and a Test Accuracy Score of 0.963 (Figure 18). Additionally, well 1054797704 recorded a Training Accuracy Score of 0.984 and a Test Accuracy Score of 0.956 (Figure 19).

For the GR log, well 1054146917 showed a Training Accuracy Score of 0.968 and a Test Accuracy Score of 0.927 (Figure 20). Meanwhile, well 1054357764 achieved a Training Accuracy Score of 0.946 and a Test Accuracy Score of 0.93 (Figure 21).

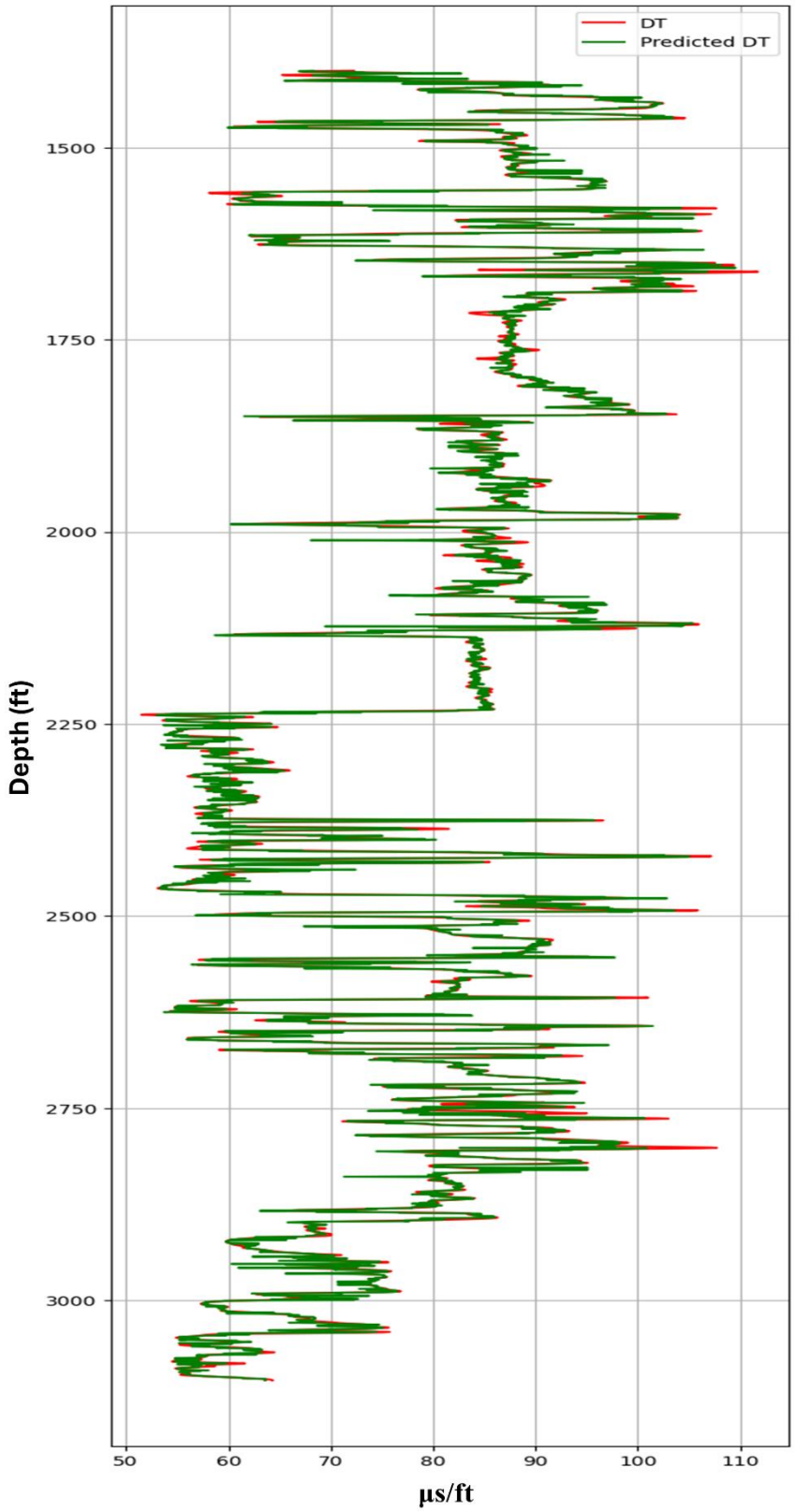

412 Figure 17: Actual vs. Predicted DT Log Responses for Well 1054310680

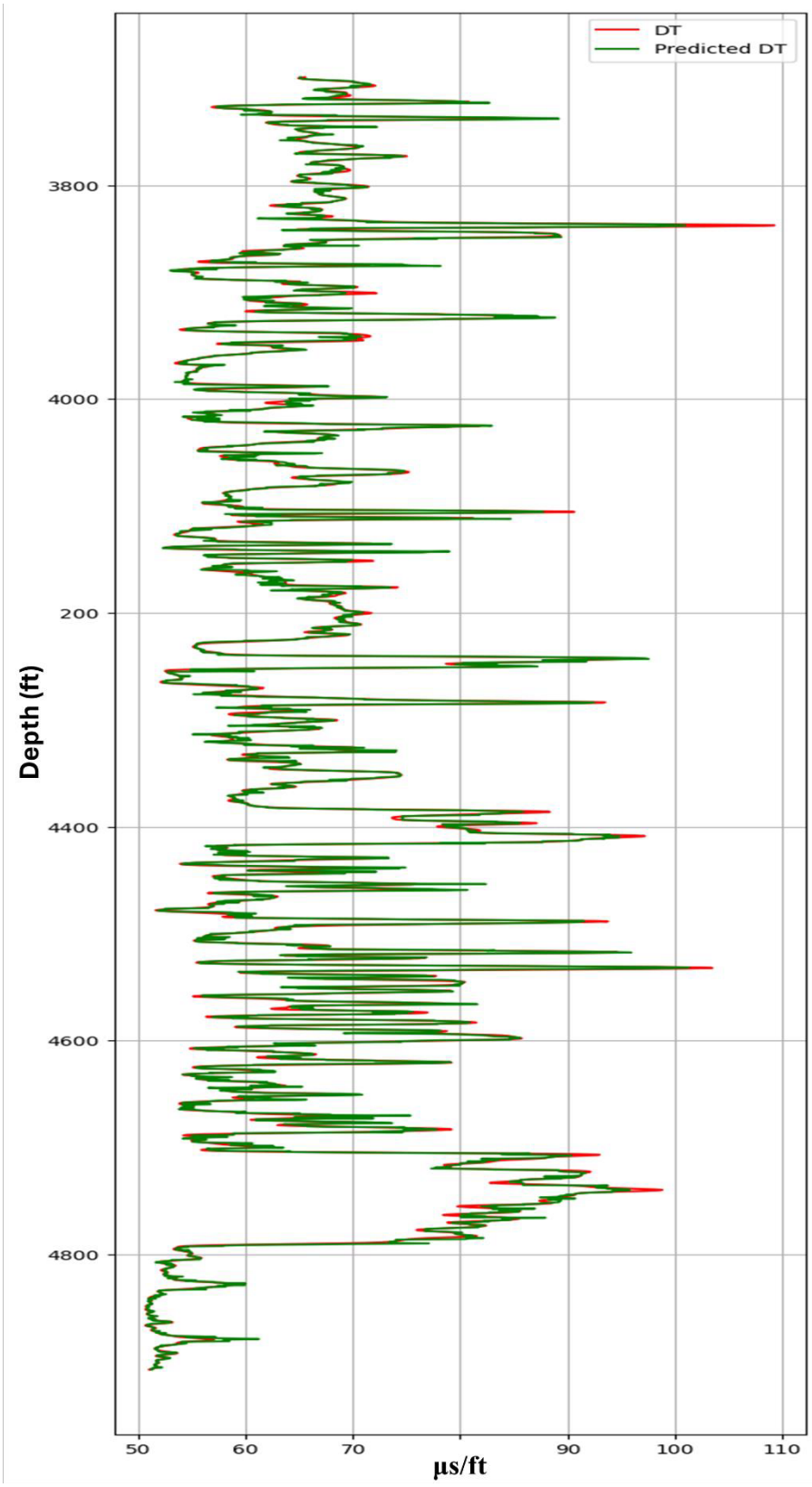

Figure 18: Actual vs. Predicted DT Log Responses for Well 1054310699.

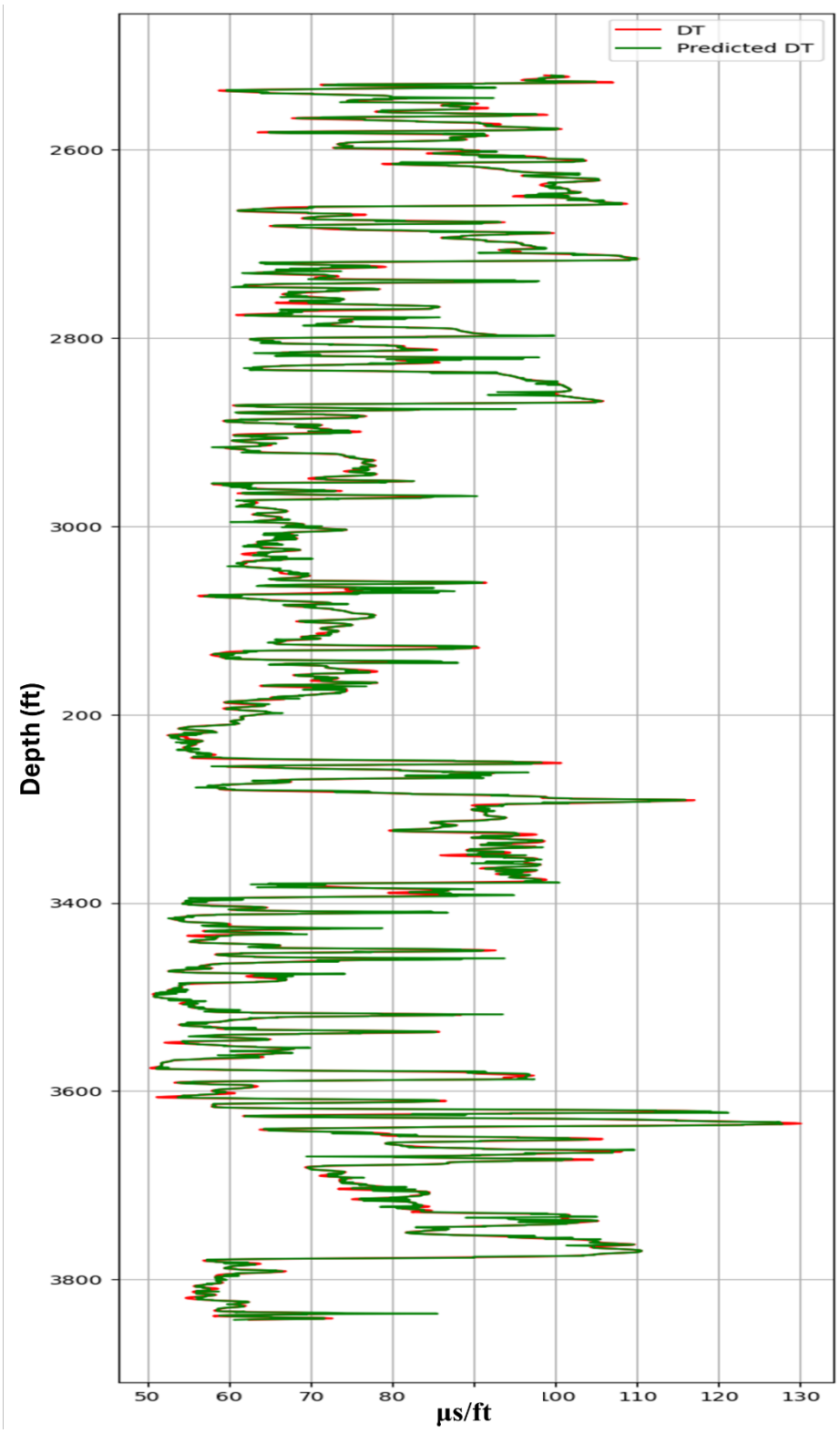

Figure 19: Actual vs. Predicted DT Log Responses for Well 1054797704

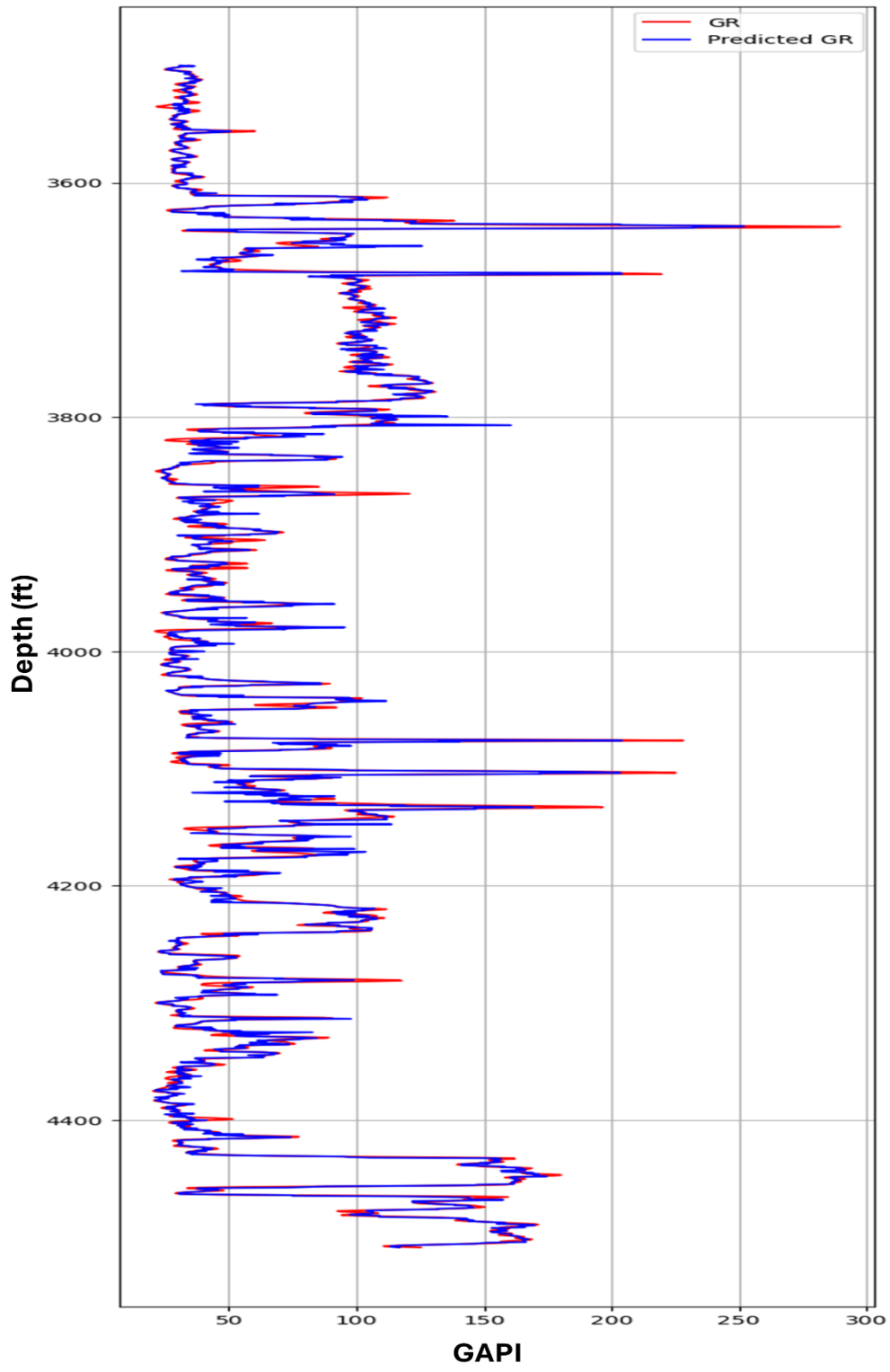

Figure 20: Actual vs. Predicted GR Log Responses for Well 1054146917.

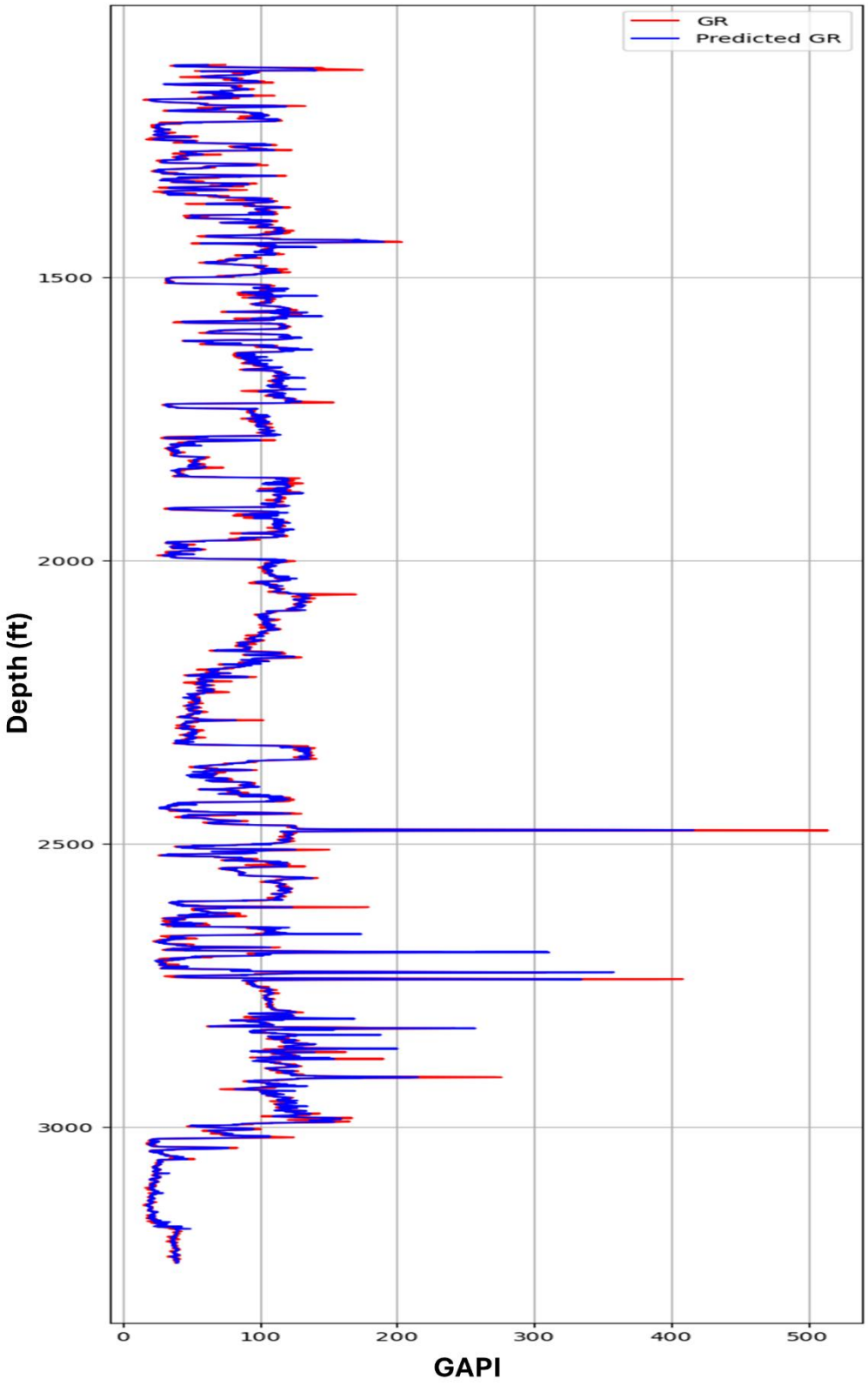

420

421 *Figure 21: Actual vs. Predicted GR Log Responses for Well* 1054357764.

4. Discussion

The results demonstrate the effective performance of KNN regression model in predicting DT and GR log responses across the evaluated wells. The high range of test accuracy scores (0.942 to 0.963 for DT and 0.927 to 0.930 for GR) indicates that the model generalizes well to unseen data, showing reliable performance for both log types. However, minor deviations were observed at certain depths, which may suggest slight inaccuracies in the model's predictions. Additionally, there are indications of minor overfitting, as evidenced by the training accuracy being higher than the test accuracy, with differences ranging from 1.69% to 4.24%.

Overfitting occurs when a model captures noise or irrelevant details from the training data, hindering its ability to generalize to new, unseen data. This issue is especially prevalent when working with small or noisy datasets, where the model can easily memorize specific patterns, exceptions, or errors within the data. For example, in the case of the dataset well 1054146917, which contains only 2,018 data points and exhibits a high overfitting rate of 4.24%, the model performs well on the training set but struggles with poor test accuracy. To mitigate overfitting, techniques such as synthetic data generation, data augmentation, and anomaly detection can be used to increase the dataset’s diversity and remove noisy points. Despite these small discrepancies, the model shows strong performance on the test data, suggesting that the overfitting is not significant. This minor variation indicates a good ability to generalize, making the model effective for predicting both DT and GR values. Overall, they demonstrate a good ability to generalize, making them effective for predicting DT and GR values.

Notably, the DT model exhibits higher test accuracy compared to the GR model. This disparity can be attributed to several factors. The features used in the DT prediction display a higher Pearson correlation coefficient with the target variable compared to those utilized for the GR prediction. Moreover, the DT model benefits from a larger dataset, providing more data points for training and evaluation. This increased volume of data enhances the model's ability to learn complex patterns and improves its predictive capability. Collectively, these factors contribute to the DT model's superior performance in comparison to the GR model.

While the model demonstrates strong performance on the tested wells, its ability to generalize to other datasets or well types may be limited due to variations in noise levels, feature

relevance, and data availability. In geophysical applications, Artificial intelligence and machine learning techniques show great potential in uncovering complex, nonlinear relationships in geophysical logs (Mukherjee et al., 2024a; Wu et al., 2018). However, their effectiveness is often constrained by small datasets, noisy inputs, and issues like overfitting. These limitations highlight the need for deep learning to enhance robustness, accuracy, and generalizability, especially when dealing with larger and more complex datasets (Yang et al., 2022; Mukherjee et al., 2024c)

5. Conclusion

This research successfully demonstrated the application of the KNN regression algorithm for predicting missing well logs, specifically DT and GR logs, across multiple wells. Utilizing an open-source dataset obtained from the University of Kansas. Optimal k values were carefully selected for each well using the RMSE metric, effectively balancing error and generalization. The KNN model achieved high test accuracy R^2 scores, ranging from 0.942 to 0.963 for DT and 0.927 to 0.930 for GR, confirming the model's robustness and capacity to generalize to unseen data. The observed differences in performance between the DT and GR models highlight how feature correlation and dataset size can impact predictive accuracy. The DT model outperformed the GR model, attributed to stronger feature correlation and a larger dataset, which provided richer training data and improved its capacity to learn complex patterns. Additionally, minor overfitting was observed, with training accuracy exceeding test accuracy by up to 4.24%; however, this difference is minimal and does not significantly affect the model's predictive capabilities. Overall, the KNN regression algorithm provides higher precision in addressing the challenges associated with missing well-log data prediction.

6. Acronyms

- **ABHV**: Apparent Bulk Hydrocarbon Volume
- **ANN**: Artificial Neural Networks
- **BRNN**: Bidirectional Recurrent Neural Networks
- **CDDPM**: Conditional Denoising Diffusion Probabilistic Model
- **CEC**: Cross-Entropy Clustering

- **CILD**: Conductivity Induction Log Deep
- **CILM**: Conductivity Induction Log Medium
- **CLL3**: Conductivity Laterolog Log 3
- **CNN**: Convolutional Neural Networks
- **ConvLSTM**: Convolutional Long Short-Term Memory
- **CNPOR**: Core Porosity
- **DT**: Delta T
- **DPOR**: Density Porosity
- **FCNN**: Fully Connected Neural Networks
- **GA**: Genetic Algorithms
- **GAPI**: Gamma Ray API Units
- **GMM**: Gaussian Mixture Model
- **GR**: Gamma Ray
- **HMM**: Hidden Markov Model
- **ICA**: Imperialist Competitive Algorithms
- **ITT**: Inter-Train Time
- **KNN**: K-Nearest Neighbors
- **LSTM**: Long Short-Term Memory
- **MEL15**: Microresistivity Log 15
- **MEL20**: Microresistivity Log 20
- **MELCAL**: Microcaliper Log
- **PSO**: Particle Swarm Optimization
- **PU**: Porosity Units

- **RILD**: Laterolog Resistivity Deep
- **RILM**: Laterolog Resistivity Medium
- **RLL3**: Lateral Log Resistivity 3
- **RNN**: Recurrent Neural Networks
- **RHOB**: Bulk Density
- **RHOC**: Core Density
- **RXORT**: Resistivity at Shallow Depth
- **SP**: Spontaneous Potential
- **SPOR**: Secondary Porosity
- **TBHV**: Total Bulk Hydrocarbon Volume

Data availability

The dataset employed in this study was obtained from the University of Kansas and is available via this link.

Disclosure of Interest

The authors declare that they have no competing interests.

7. References

Ali, P. J. M. (2022). Investigating the Impact of min-max data normalization on the regression performance of K-nearest neighbor with different similarity measurements. *ARO-The Scientific Journal of Koya University*, *10*(1), 85-91.https://doi.org/10.14500/aro.10955

Alward, W., Al-Jubouri, M., Zongfa, L., Xiaori, X., Wei, X., & Yufang, Z. (2023). Automated Well Log Interpretation Through Machine Learning. In *SPE Gas & Oil Technology Showcase and Conference* (p. D021S016R005). SPE. https://doi.org/10.2118/214055-ms

Barbosa, M. R. S., Carneiro, V., & Cerqueira, A. G. (2022). Seismic Well Tie using Geophysical Logs obtained from K-Nearest Neighbor Regression Algorithm. *Brazilian Journal of Geophysics*, *40*(1). https://doi.org/10.22564/brjg.v40i1.2157

Benedetti, J. K. (1977). On the nonparametric estimation of regression functions. *Journal of the Royal Statistical Society: Series B (Methodological)*, *39*(2), 248-253.

Feng, R., Grana, D., & Balling, N. (2021). Imputation of missing well log data by random forest and its uncertainty analysis. *Computers & Geosciences*, *152*, 104763. https://doi.org/10.1016/j.cageo.2021.104763

Gholamy, A., Kreinovich, V., & Kosheleva, O. (2018). *Why 70/30 or 80/20 relation between training and testing sets: A pedagogical explanation*. Departmental Technical Reports (CS), 1209. University of Texas at El Paso. https://scholarworks.utep.edu/cs_techrep/1209

Gómez, F., Flores, Y., & Vadászi, M. (2022). Comparative analysis of the K-nearest-neighbour method and K-means cluster analysis for lithological interpretation of well logs of the Shushufindi Oilfield, Ecuador. *Rudarsko-geološko-naftni zbornik*, *37*(4), 155-165.https://doi.org/10.17794/rgn.2022.4.13

Goyal, R., Chandra, P., & Singh, Y. (2014). Suitability of KNN Regression in the Development of Interaction based Software Fault Prediction Models. *IERI Procedia, 6,* 15–21. https://doi.org/10.1016/j.ieri.2014.03.004

Grčar, M., Mladenič, D., Fortuna, B., & Grobelnik, M. (2006). Data sparsity issues in the collaborative filtering framework. In *Advances in Web Mining and Web Usage Analysis: 7th International Workshop on Knowledge Discovery on the Web, WebKDD 2005, Chicago, IL, USA, August 21, 2005. Revised Papers 7* (pp. 58-76). Springer Berlin Heidelberg. https://doi.org/10.1007/11891321_4

Henderi, H., Wahyuningsih, T., & Rahwanto, E. (2021). Comparison of Min-Max normalization and Z-Score Normalization in the K-nearest neighbor (kNN) Algorithm to Test the Accuracy of Types of Breast Cancer. *International Journal of Informatics and Information Systems*, *4*(1), 13-20. https://doi.org/10.47738/ijiis.v4i1.73

Hu, C., Jain, G., Zhang, P., Schmidt, C., Gomadam, P., & Gorka, T. (2014). Data-driven method based on particle swarm optimization and k-nearest neighbor regression for estimating capacity of lithium-ion battery. *Applied Energy*, *129*, 49–55. https://doi.org/10.1016/j.apenergy.2014.04.077

Kim, M. J., & Cho, Y. (2024). Imputation of missing values in well log data using k-nearest neighbor collaborative filtering. *Computers & Geosciences*, *193*, 105712. https://doi.org/10.1016/j.cageo.2024.105712

Kramer, O. (2011). Dimensionality reduction by unsupervised k-nearest neighbor regression. In *2011 10th international conference on machine learning and applications and workshops* (Vol. 1, pp. 275-278). IEEE. **https://doi.org/10.1109/icmla.2011.55**

Kumar, V., & Reinartz, W. (2014). Commercial data mining: Processing, analysis and modeling for predictive analytics projects (pp. 79-104). In *Data mining and knowledge discovery handbook* (2nd ed.). Elsevier. https://doi.org/10.1016/B978-012416602-8.00006-6

Mailagaha Kumbure, M., & Luukka, P. (2022). A generalized fuzzy k-nearest neighbor regression model based on Minkowski distance. *Granular Computing*, *7*(3), 657-671. https://doi.org/10.1007/s41066-021-00288-w

Mukherjee, B., Gautam, Param. K., & Sain, K. (2024a). Machine learning assisted crustal velocity proxy: A case study over the Tibetan Plateau and its surroundings. *Journal of Asian Earth Sciences*, *263*, 106004. https://doi.org/10.1016/j.jseaes.2023.106004

Mukherjee, B., Sain, K., Kar, S., & V, S. (2024b). Deep learning-aided simultaneous missing well log prediction in multiple stratigraphic units: a case study from the Bhogpara oil field, Upper Assam, Northeast India. *Earth Science Informatics, 17*(5), 4901-4929. https://doi.org/10.1016/j.jseaes.2023.106004

Meng, H., Lin, B., Zhang, R., & Jin, Y. (2024). A Missing Well-Logs Imputation Method Based on Conditional Denoising Diffusion Probabilistic Models. *SPE Journal*, *29*(05), 2165–2180. https://doi.org/10.2118/219452-pa

Nettleton, D. (2014). Pearson correlation - An overview. In *Commercial data mining: Processing, analysis and modeling for predictive analytics projects* (pp. 79-104). Elsevier.

Pan, R., Yang, T., Cao, J., Lu, K., & Zhang, Z. (2015). Missing data imputation by K nearest neighbours based on grey relational structure and mutual information. *Applied Intelligence*, *43*(3), 614–632. https://doi.org/10.1007/s10489-015-0666-x

Pham, N., Wu, X., & Ehsan Zabihi Naeini. (2020). Missing well log prediction using convolutional long short-term memory network. *Geophysics*, *85*(4), WA159–WA171. https://doi.org/10.1190/geo2019-0282.1

Picard, R. R., & Berk, K. N. (1990). Data Splitting. *The American Statistician*, *44*(2), 140–147. https://doi.org/10.2307/2684155

Prajapati, R., Mukherjee, B., Singh, U. K., & Sain, K. (2024). Machine learning assisted lithology prediction using geophysical logs: A case study from Cambay basin. *Journal of Earth System Science*, *133*(2). https://doi.org/10.1007/s12040-024-02326-y

Qiao, L., Cui, Y., Jia, Z., Xiao, K., & Su, H. (2022). Missing Well Logs Prediction Based on Hybrid Kernel Extreme Learning Machine Optimized by Bayesian Optimization. *Applied Sciences*, *12*(15), 7838–7838. https://doi.org/10.3390/app12157838

Rahmati, M., Zargar, G., & Ayatizadeh Tanha, A. (2024). Predicting density log from well log using machine learning techniques and heuristic optimization algorithm: A comparative study. *Petroleum Research, 9*(2), 176–192. https://doi.org/10.1016/j.ptlrs.2024.01.008

Raykar, V. C., & Saha, A. (2015). Data split strategies for evolving predictive models. In *Machine Learning and Knowledge Discovery in Databases: European Conference, ECML PKDD 2015, Porto, Portugal, September 7-11, 2015, Proceedings, Part I 15* (pp. 3-19). Springer International Publishing.

Salehi, M. M., Rahmati, M., Karimnezhad, M., & Omidvar, P. (2017). Estimation of the non records logs from existing logs using artificial neural networks. *Egyptian Journal of Petroleum*, *26*(4), 957-968.10.1016/j.ejpe.2016.11.002

Shchutskaya, V. (2021). *What is predictive performance models and why their performance evaluation is important*. Retrieved from https://indatalabs.com/blog/predictive-models-performance-evaluation-important

Srisuradetchai, P., & Suksrikran, K. (2024). Random kernel k-nearest neighbors regression. *Frontiers in Big Data, 7*, 1402384. https://doi.org/10.3389/fdata.2024.1402384

Stone, C. J. (1977). Consistent Nonparametric Regression. *The Annals of Statistics*, *5*(4), 595–620. https://www.jstor.org/stable/2958783

Song, Y., Liang, J., Lu, J., & Zhao, X. (2017). An efficient instance selection algorithm for k nearest neighbor regression. *Neurocomputing*, *251*, 26–34. https://doi.org/10.1016/j.neucom.2017.04.018

Turney, S. (2022). Pearson correlation coefficient (r) | Guide & examples. Scribbr. Retrieved from https://www.scribbr.com/statistics/pearson-correlation-coefficient/

Wilcox, R. R. (2003). Probability and related concepts. In *Applying contemporary statistical techniques* (pp. 17-53). Elsevier. https://doi.org/10.1016/b978-012751541-0/50023-7

Wu, L., Dong, Z., Li, W., Jing, C., & Qu, B. (2021). Well-Logging Prediction Based on Hybrid Neural Network Model. *Energies*, *14*(24), 8583. https://doi.org/10.3390/en14248583

Wu, P. Y., Jain, V., Kulkarni, M. S., & Abubakar, A. (2018). Machine learning-based method for automated well-log processing and interpretation. In *SEG International Exposition and Annual Meeting* (pp. SEG-2018). SEG. https://doi.org/10.1190/segam2018-2996973.1

Yang, L., Wang, S., Chen, X., Chen, W., Saad, O. M., & Chen, Y. (2022). Deep-learning missing well-log prediction via long short-term memory network with attention-period mechanism. *Geophysics, 88*(1), D31–D48. https://doi.org/10.1190/geo2020-0749.1

Zhang, D., Yuntian, C. H. E. N., & Jin, M. E. N. G. (2018). Synthetic well logs generation via Recurrent Neural Networks. *Petroleum Exploration and Development*, *45*(4), 629-639. https://doi.org/10.1016/s1876-3804(18)30068-5